AUTOPHAGY
https://doi.org/10.1080/15548627.2021.1971937

Taylor & Francis
Taylor & Francis Group

RESEARCH PAPER

DYNC1LI2 regulates localization of the chaperone-mediated autophagy receptor LAMP2A and improves cellular homeostasis in cystinosis

Farhana Rahman[a], Jennifer L. Johnson[a], Jinzhong Zhang[a], Jing He[a], Kersi Pestonjamasp[a], Stephanie Cherqui[b], and Sergio D. Catz [a]

[a]Department of Molecular Medicine, The Scripps Research Institute, La Jolla, CA, USA; [b]Department of Pediatrics, University of California San Diego, La Jolla, CA, USA

ABSTRACT

The dynein motor protein complex is required for retrograde transport but the functions of the intermediate-light chains that form the cargo-binding complex are not elucidated and the importance of individual subunits in maintaining cellular homeostasis is unknown. Here, using mRNA arrays and protein analysis, we show that the dynein subunit, DYNC1LI2 (dynein, cytoplasmic 1 light intermediate chain 2) is downregulated in cystinosis, a lysosomal storage disorder caused by genetic defects in CTNS (cystinosin, lysosomal cystine transporter). Reconstitution of DYNC1LI2 expression in *ctns*$^{-/-}$ cells reestablished endolysosomal dynamics. Defective vesicular trafficking in cystinotic cells was rescued by DYNC1LI2 expression which correlated with decreased endoplasmic reticulum stress manifested as decreased expression levels of the chaperone HSPA5/GRP78, and the transcription factors ATF4 and DDIT3/CHOP. Mitochondrial fragmentation, membrane potential and endolysosomal-mitochondrial association in cystinotic cells were rescued by DYNC1LI2. Survival of cystinotic cells to oxidative stress was increased by DYNC1LI2 reconstitution but not by its paralog DYNC1LI1, which also failed to decrease ER stress and mitochondrial fragmentation. DYNC1LI2 expression rescued the localization of the chaperone-mediated autophagy (CMA) receptor LAMP2A, CMA activity, cellular homeostasis and LRP2/megalin expression in cystinotic proximal tubule cells, the primary cell type affected in cystinosis. DYNC1LI2 failed to rescue phenotypes in cystinotic cells when LAMP2A was downregulated or when co-expressed with dominant negative (DN) RAB7 or DN-RAB11, which impaired LAMP2A trafficking. DYNC1LI2 emerges as a regulator of cellular homeostasis and potential target to repair underlying trafficking and CMA in cystinosis, a mechanism that is not restored by lysosomal cystine depletion therapies.

Abbreviations: ACTB: actin, beta; ATF4: activating transcription factor 4; CMA: chaperone-mediated autophagy; DYNC1LI1: dynein cytoplasmic 1 light intermediate chain 1; DYNC1LI2: dynein cytoplasmic 1 light intermediate chain 2; ER: endoplasmic reticulum; LAMP1: lysosomal associated membrane protein 1; LAMP2A: lysosomal associated membrane protein 2A; LIC: light-intermediate chains; LRP2/Megalin: LDL receptor related protein 2; PTCs: proximal tubule cells; RAB: RAB, member RAS oncogene family; RAB11FIP3: RAB11 family interacting protein 3; RILP: Rab interacting lysosomal protein

ARTICLE HISTORY
Received 10 July 2020
Revised 13 August 2021
Accepted 18 August 2021

KEYWORDS
Lysosomal storage disorder; megalin; proximal tubule cell; rab gtpases; trafficking

Introduction

Cystinosis is a lysosomal storage disorder caused by the accumulation of the amino acid cystine due to genetic defects in the *CTNS* gene, which encodes the lysosomal cystine transporter [1,2]. Increased levels of intra-lysosomal cystine lead to cell malfunction, which is especially manifested in the kidney's epithelial proximal tubule cells (PTCs). However, many cellular defects in cystinosis are independent of lysosomal overload [3–5], suggesting that CTNS regulates cellular processes independently of its role as a cystine transporter. The efficiency of cysteamine in retarding the rate of glomerular deterioration and improvement of linear growth in children with cystinosis demonstrates the effectiveness of cystine-depleting therapies [6–8]. However, even with cysteamine treatment, cell malfunction, tissue failure and progressive renal injury still occurs [9], thus, cystine accumulation is not the only cause of all the defects observed in cystinosis [9,10]. Although the molecular defects that initiate or promote disease progression in cystinosis are not fully characterized, several lines of evidence point to defects in vesicular trafficking as one of the molecular mechanisms that are defective in cystinosis but not repaired by cysteamine [11,12].

Dynein, a large motor protein complex, carries out an extensive range of cellular processes. The dynein family includes axonemal dyneins that drive ciliary and flagellar motility [13] and cytoplasmic dyneins which perform several intracellular processes including cargo transport, organelle trafficking and mitotic spindle assembly and positioning [14,15]. Dynein controls cellular functions through regulatory movement to the minus-end of the microtubules, a process referred to as retrograde transport. Cytoplasmic dynein complexes are composed of dynein intermediate chains, light-intermediate chains (LIC) and light chains, which form

CONTACT Sergio D. Catz scatz@scripps.edu Department of Molecular Medicine, The Scripps Research Institute, 10550 North Torrey Pines Road, La Jolla, CA, 92037

a complex with two identical subunits of dynein heavy chains [16]. The complex is regulated by dynactin and adaptor proteins [17–19], which facilitate the movement along microtubules [20], but how dynein light chain subunits help perform individual cellular functions is not completely understood.

Individual dynein subunits may allow specific functions and interactions with specific binding partners that regulate dynein motor activity [18]. While the dynein heavy chain polypeptides provide the energy that facilitates movement along microtubules, the functional roles of the intermediate, light-intermediate, and light chain polypeptides remain poorly understood. The dynein LIC subunits present in cytoplasmic dyneins are proposed to regulate cargo attachment and dynein transport [21–24]. The two genes *DYNC1LI1* (dynein cytoplasmic 1 light intermediate chain 1) and *DYNC1LI2* show 63% sequence identity in humans and share high sequence similarity within the dynein- and cargo-binding domains [25,26].

DYNC1LI1 and DYNC1LI2 were found to perform overlapping functions in cells in earlier studies [27]. However, a recent work demonstrated that both LICs have distinct roles in neurogenesis, migration, and translocation [25,28]. Mammalians LICs bind to GDP *via* their RAS-like G-domain, which may be released upon binding to the dynein heavy chain [29]. Furthermore, the C-terminal domain of DYNC1LI1 has been shown to bind directly to RILP (Rab interacting lysosomal protein) [30], RAB11FIP3 (RAB11 family interacting protein 3) [31,32] and BICD2 (BICD cargo adaptor 2) [18,33], which are effector molecules of the RAB GTPases RAB7, RAB11 and RAB6, respectively. Thus, LICs bridge the motor heavy chain to specific vesicle-associated molecular effectors, and thus may contribute to the control of the specificity of cargoes during retrograde transport.

Autophagy is a regulated cellular mechanism of degradation of cytoplasmic material in lysosomes, that contributes to nutrient preservation and maintains cellular homeostasis. Chaperone-mediated autophagy (CMA) [34] is a selective form of autophagy consisting of the chaperone-dependent selection of soluble cytosolic proteins with a KFERQ-like signal peptide that are then targeted to lysosomes and directly translocated across the lysosome membrane for degradation [35]. The targeted substrate-chaperone complex binds to the lysosomal surface through the cytosolic tail of the LAMP2A (lysosomal associated membrane protein 2A) [36], the only CMA receptor. Similar to macroautophagy, CMA upregulation occurs during prolonged nutritional stress (starvation), exposure to toxic compounds, and mild oxidative stress [37] suggesting a role for this pathway in the selective removal of abnormal or damaged proteins under these conditions [38]. In previous studies, we revealed a defective mechanism of CMA in cystinosis [3,11,39]. In particular, we showed defective trafficking and mislocalization of the CMA receptor LAMP2A in cystinosis, a process associated with impaired cellular homeostasis manifested as increased endoplasmic reticulum stress and decreased survival to oxidative stress [3]. Furthermore, we established that correct LAMP2A localization depends on trafficking mechanisms regulated by the small GTPases RAB11 and RAB7 [11].

Here, to better understand the mechanisms underlying vesicular transport defects in cystinosis, we used an mRNA array approach and identified the motor protein subunit dynein light intermediate chain DYNC1LI2 to be downregulated in cystinosis. Rescue of DYNC1LI2 expression increases LAMP2A trafficking and improves cell homeostasis in both cystinotic fibroblast and proximal tubule epithelial cells. Mechanistically, the rescue of cystinotic cell function by DYNC1LI2 requires functional RAB11 and RAB7 GTPases, and the process is inhibited by downregulation of LAMP2A. Thus, DYNC1LI2 regulates vesicular trafficking and lysosomal-associated protein sorting through a mechanism controlled by chaperone-mediated autophagy and is essential to restore cellular homeostasis in cystinosis.

Results

DYNC1LI2 is downregulated in cystinotic cells

Vesicular trafficking is defective in cystinosis [12]. To identify potential molecular regulators of vesicular trafficking that are dysregulated in cystinosis, we performed mRNA analysis of cystinotic kidneys. Analysis based on differentially expressed genes (DEGs) between 6 wild-type and 6 *ctns*$^{-/-}$ kidney samples identified 3260 DEGs from 28,853 genes analyzed using the BRB-ArrayTools (Table S1) and depicted in heatmap (Figure 1A, ROSALIND™). Based on our previous knowledge that the retrograde transport is defective in cystinotic proximal tubule cells, we focused on genes that mediate this transport system. Among these genes, we showed that RILP, a RAB7 effector shown by our group to regulate vesicular trafficking in cystinosis and to be downregulated in cystinotic fibroblast at the RNA and protein levels [11], is also downregulated in *ctns*$^{-/-}$ kidney. Next, we focused on dyneins, which are known regulators of the retrograde transport system. Here, we identified DYNC1LI2, a light intermediate subunit of the motor protein dynein to be significantly downregulated in six independent cystinosis kidney samples (Figure 1B). Contrary, a group of kinesin family members, motor proteins that regulate the anterograde transport, were upregulated in cystinotic kidneys (Figure 1B and Table S1). Because DYNC1LI2 is downregulated in cystinosis, DYNC1LIs interact with RILP [40], and RILP is also downregulated in cystinosis, we identify DYNC1LI2 as a potential important trafficking regulatory molecule in cystinosis and selected DYNC1LI2 for downstream analysis.

Quantitative analysis of mRNA levels for *Dync1li2* in mouse embryonic fibroblasts (MEFs) show significant decreased levels in *ctns*$^{-/-}$ cells thus corroborating the results obtained in kidneys by RNA arrays (Figure 1C). DYNC1LI2 downregulation at the protein level in cystinosis was confirmed by immunoblotting of WT and *ctns*$^{-/-}$ MEFs (Figure 1D). Quantitative immunoblotting analysis shows that DYNC1LI2 expression is significantly decreased in cystinotic cells compared to wild-type cells (Figure 1E). As control, cystinotic cells were routinely checked for lysosomal overload using mass spectrometry analysis of accumulated cystine as described [3] (Figure S1). Cystine accumulation in cystinosis was not decreased by DYNC1LI2 expression (data

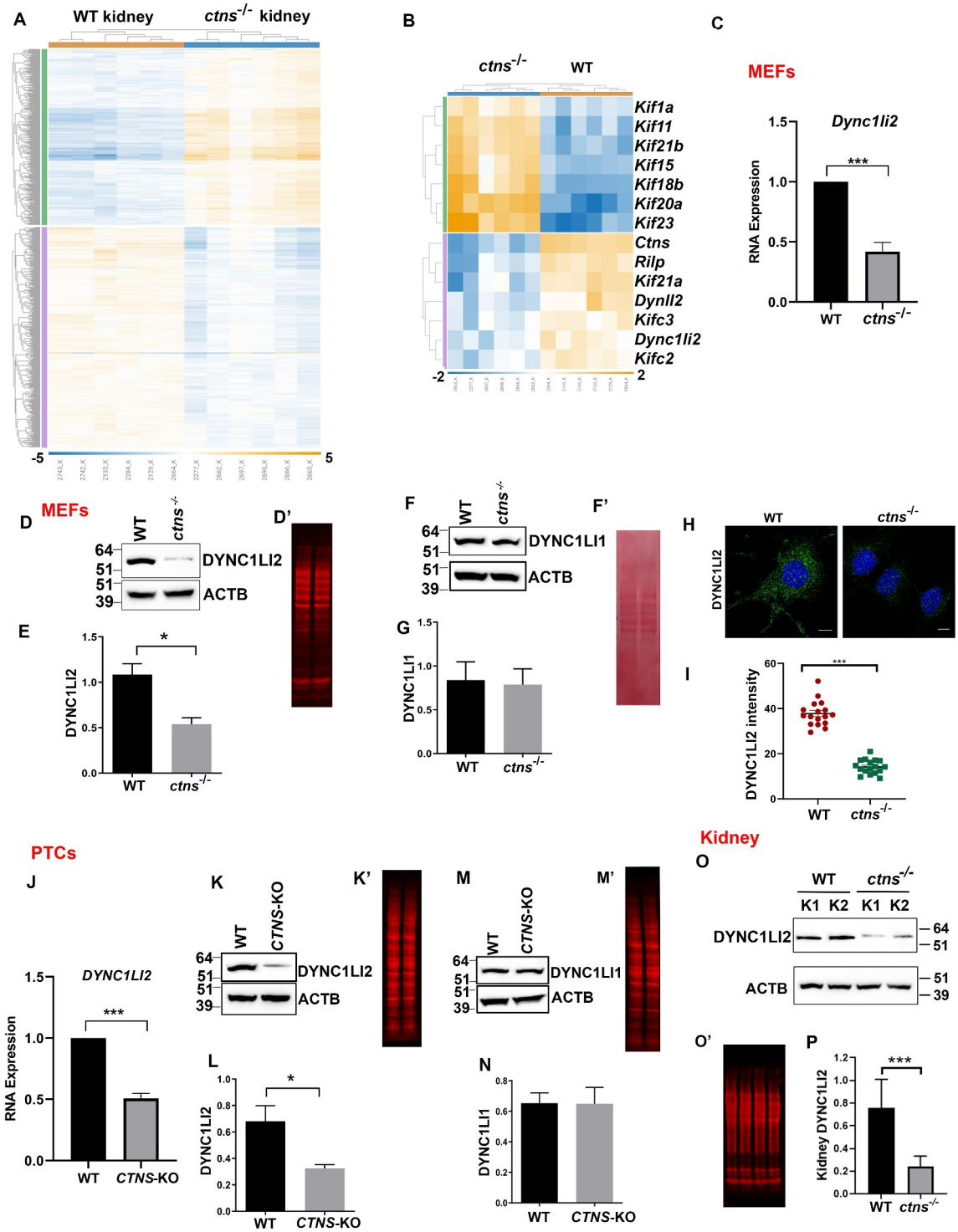

Figure 1. DYNC1LI2 but not DYNC1LI1 is downregulated in cystinosis. (A and B) Heatmap representations of differential gene expression analysis in kidneys from WT and *ctns*$^{-/-}$ mice. The differentially expressed genes (DEGs) identified in 6 wild-type and 6 *ctns*$^{-/-}$ kidney samples, are presented in associated Table S1. (B) Analysis of up- and downregulated genes in WT and *ctns*$^{-/-}$ kidneys using The OnRamp BioInformatic platform ROSALIND™ confirmed that several retrograde transport system-associated genes are downregulated, while several proteins from the kinesin family are upregulated in cystinosis. (C) Quantification of *Dync1li2* mRNA levels from four independent samples of WT and *ctns*$^{-/-}$ fibroblasts using real-time PCR, confirmed *Dync1li2* downregulation in cystinosis. (D) Expression of DYNC1LI2 in WT and *ctns*$^{-/-}$ fibroblasts was analyzed by western blot using ACTB and total protein (D') as controls. (E) Quantification of DYNC1LI2 expression levels from 3 independent experiments. (F) Expression of DYNC1LI1 in WT and *ctns*$^{-/-}$ mouse fibroblasts analyzed by western blot. (G) Quantification of DYNC1LI1 expression levels from 3 independent experiments. (H and I) Immunofluorescence analysis of DYNC1LI2 expression in wild-type and *ctns*$^{-/-}$ MEFs. Scale bar: 10 µm. Quantification of DYNC1LI2 fluorescence intensity (RFU). Each symbol represents the average fluorescence intensity of the cells per field. A total of 17 fields and 30 to 35 cells were quantified for WT and *ctns*$^{-/-}$ cells, respectively, in 3 independent experiments. (J) Real-time PCR analysis of *DYNC1LI2* RNA expression in wild type and *CTNS-KO* proximal tubule cells (PTCs) from three independent samples. (K and L) Expression of DYNC1LI2 in WT and *CTNS*-KO human PTCs analyzed by western blot from 3 independent experiments. (M and N) Expression of DYNC1LI1 in WT and *CTNS*-KO human PTCs analyzed by western blot from 3 independent experiments. (O and P) Quantitative immunoblotting showing decreased DYNC1LI2 expression in kidney lysates from cystinotic (*ctns*$^{-/-}$) mice. (O) Two representative kidneys are shown. (P) (n = 6 samples from independent mice). (D' to O') total protein loading controls. Mean ± SEM *, $p < 0.05$, ***, $p < 0.001$.

not shown). As an additional control, we examined the expression of the DYNC1LI1 subunit, a paralog of DYNC1LI2. Unlike DYNC1LI2, the expression of DYNC1LI1 in *ctns*$^{-/-}$ cells was no different from that observed in wild-type cells (Figure 1F,G). The selective decreased expression of DYNC1LI2 was also confirmed using an independent approach consisting of the immunofluorescence analysis of endogenous DYNC1LI2 protein (Figure 1H,I). Next, we engineered CRISPR-Cas9 cystinotic human proximal tubule cells (*CTNS*-KO PTCs) [39] which, similar to *ctns*$^{-/-}$ fibroblasts, expressed significantly decreased levels of *Dync1li2* mRNA (Figure 1J) and DYNC1LI2 protein (Figure 1K,L), but normal levels of the paralog DYNC1LI1 (Figure 1M,N). Finally, decreased DYNC1LI2 protein expression was confirmed in independent kidney samples from *ctns*$^{-/-}$ mice (Figure 1O,P).

DYNC1LI2 rescues vesicular trafficking and the localization of the CMA receptor, LAMP2A, in cystinosis

Cystinotic cells are characterized by impaired vesicular trafficking mechanisms that have deleterious consequences on cell homeostasis and function [11,12]. In this work, to analyze whether reconstitution of DYNC1LI2 expression rescues the vesicular transport impaired phenotypes and associated defects in cystinotic cells, we stably reconstituted DYNC1LI2 expression or, as control, stably expressed DYNC1LI1 in *ctns*$^{-/-}$ cells by lentiviral infection. Next, to analyze the impact of DYNC1LI2 reconstitution on vesicular dynamics in *ctns*$^{-/-}$ cells, we first studied endolysosomal trafficking in cells labeled with the acidotropic dye LysoTracker, by Total Internal Reflection Fluorescence microscopy (TIRFM). We found that the dynamics of vesicles in *ctns*$^{-/-}$ cells was significantly impaired compared to wild-type cells (Figure 2A,B and Movies S1 to S4). In these assays, the vesicles were segregated according to their speed, and *ctns*$^{-/-}$ cells showed increased numbers of non-motile vesicles and vesicles moving at very low speed with a concomitant decreased of fast-moving vesicles (Figure 2B). The defective phenotype was rescued by reconstitution of DYNC1LI2-expression. Next, we asked whether the exogenous expression of the paralog DYNC1LI1 also improves endolysosomal trafficking in these cells. Exogenous expression of DYNC1LI1 also rescued the defective trafficking phenotype in *ctns*$^{-/-}$ cells albeit not as efficiently as DYNC1LI2. Altogether the data support the premise that expression of DYNC1LI1/2 in *ctns*$^{-/-}$ fibroblasts reestablishes endolysosomal dynamics.

Defective CMA in cystinosis is associated with impaired LAMP2A trafficking and the CMA receptor is retained in RAB11-positive carrier vesicles in cystinotic cells, a phenotype that is rescued by the expression of constitutively active RAB11 but not by cysteamine treatment [3,11,39]. Here, we next analyzed whether DYNC1LI2 or DYNC1LI1 were able to rescue the mislocalization of the CMA receptor, LAMP2A, at lysosomes. To this end, we performed confocal microscopy analysis of the localization of LAMP2A in relation to the lysosomal marker LAMP1. We show a significantly increased colocalization of the CMA receptor LAMP2A with LAMP1-positive puncta in *ctns*$^{-/-}$ cells after reconstitution of DYNC1LI2 expression. Contrarily, DYNC1LI1 over-expression did not rescue the LAMP2A-mislocalized phenotype (Figure 2C,D), despite its partial rescue effect on endolysosomal trafficking (Figure 2A,B). Altogether, these results suggest that DYNC1LI2 but not DYNC1LI1 regulates the trafficking of LAMP2A-carrying intermediate vesicles [3], thus establishing unique mechanistic and trafficking properties for DYNC1LI2 in this cellular system.

DYNC1LI2-downregulated cells have deficient CMA and DYNC1LI2 rescues defective CMA in cystinosis

LAMP2A-mediated substrate binding and internalization are essential processes for CMA and defective LAMP2A trafficking to the lysosomal membrane impairs CMA activity in cystinosis. To test whether DYNC1LI2 downregulation resulted in impaired CMA activity, we utilized a validated assay [41,42] to assess the ability of isolated lysosomes to digest CMA substrates. Lysosomes were isolated with methods that efficiently isolate both normal lysosomes and lysosomes with cargo overload [3]. Lysosomes showed ≥85% integrity measured as the HEX/β-hexosaminidase activity in intact lysosomes compared to burst lysosomes, as described in Materials and Methods (Figures S2A and B). The enriched lysosomal fractions were free of mitochondria, ER and cytosolic contaminants (Figures S2C and D). Lysosomes from WT, *ctns*$^{-/-}$, or DYNC1LI2-reconstituted *ctns*$^{-/-}$ cells were incubated with the validated CMA substrate recombinant (r) GAPDH, in the presence of HSPA8/HSC70 (heat shock protein family A (Hsp70) member 8), under conditions compatible with substrate translocation (ATP-regeneration system) and CMA activity (full reaction) or under translocation inhibition (no ATP/energy regeneration system) or no degradation (protease inhibitors) conditions. *ctns*$^{-/-}$ cells presented impaired CMA (Figure 3), thus confirming previous studies [3]. Reconstitution of DYNC1LI2 expression partially rescued CMA activity (Figure 3A,B); thus, *ctns*$^{-/-}$ cells rescued for DYNC1LI2 expression showed significantly increased levels of CMA substrate degradation when compared to *ctns*$^{-/-}$ cells; however, the CMA activity in rescued cells was still lower than that observed in wild-type cells (Figure 3A,B, $p = 0.052$). Next, we analyzed CMA activity in lysosomes from cells in which *Dync1li2* was downregulated using shRNA technology (sh*Dync1li2*). We show that sh*Dync1li2* cells have defective CMA (Figure 3C,D), indicating that CMA activity is dependent on DYNC1LI2-mediated vesicular trafficking. Of note, the use of rGAPDH as a CMA substrate in the isolated lysosomal assay has been optimized and largely validated for the cell-free systems. Furthermore, GAPDH expression level is sensitive to long-term changes in CMA activity in cystinosis tissues (data not shown). However, endogenous GAPDH expression is not affected in short term cultured cystinotic cells, which is most likely explained by competitive exclusion by other substrates prioritized by the CMA machinery, including oxidized proteins, which are elevated in cystinosis (Figure S3).

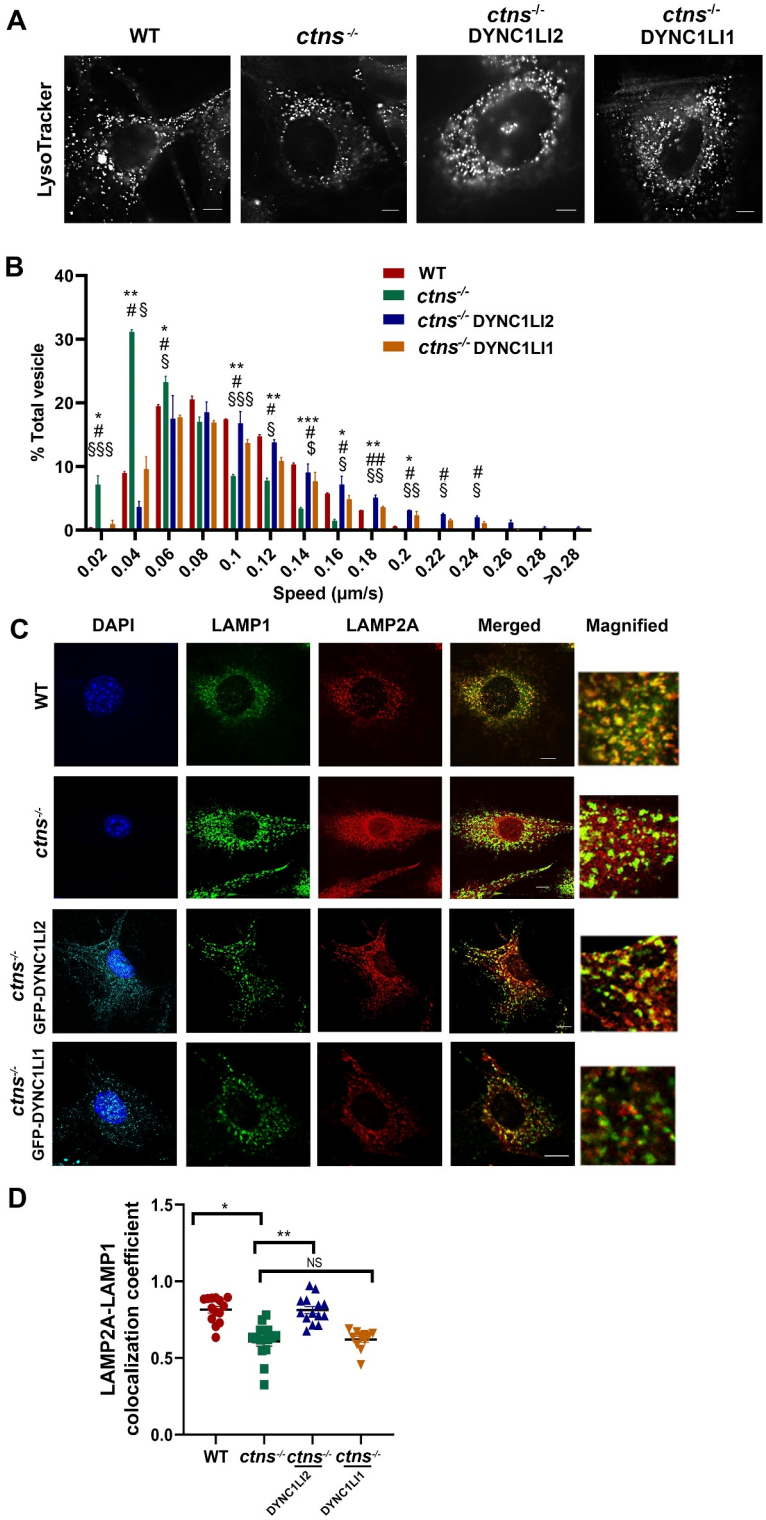

Figure 2. DYNC1LI2 rescues vesicular trafficking and lysosomal localization of LAMP2A in cystinotic cells. (A) Representative images from the analysis of vesicle movement in wild-type, *ctns*$^{-/-}$, DYNC1LI2- and DYNC1LI1-expressing *ctns*$^{-/-}$ cells by TIRFM. Scale bar: 10 µm. (B) the speeds for the independent vesicles were binned in 0.02 µm/s increments and plotted as a percentage of total vesicles for a given cell. The statistically significant differences between the groups are indicated in the figure. Mean ± SEM *, $p < 0.05$; **, $p < 0.01$; ***, $p < 0.001$, WT *vs* *ctns*$^{-/-}$. #, $p < 0.05$; # #, $p < 0.01$, *ctns*$^{-/-}$ *vs* DYNC1LI2. §, $p < 0.05$, §§, $p < 0.01$, §§§, $p < 0.001$, *ctns*$^{-/-}$ *vs* DYNC1LI1. (C) Immunofluorescence analysis of endogenous LAMP1 (pseudo-colored green) and LAMP2A (red) localization in WT, *ctns*$^{-/-}$, GFP-(pseudo-colored cyan)-DYNC1LI2-, and GFP-(cyan)-DYNC1LI1-expressing *ctns*$^{-/-}$ cells. Scale bar: 10 µm. (D) LAMP2A-LAMP1 colocalization increases in response to GFP-DYNC1LI2 expression. Mean ± SEM, *, $p < 0.05$; **, $p < 0.01$; NS, not significant.

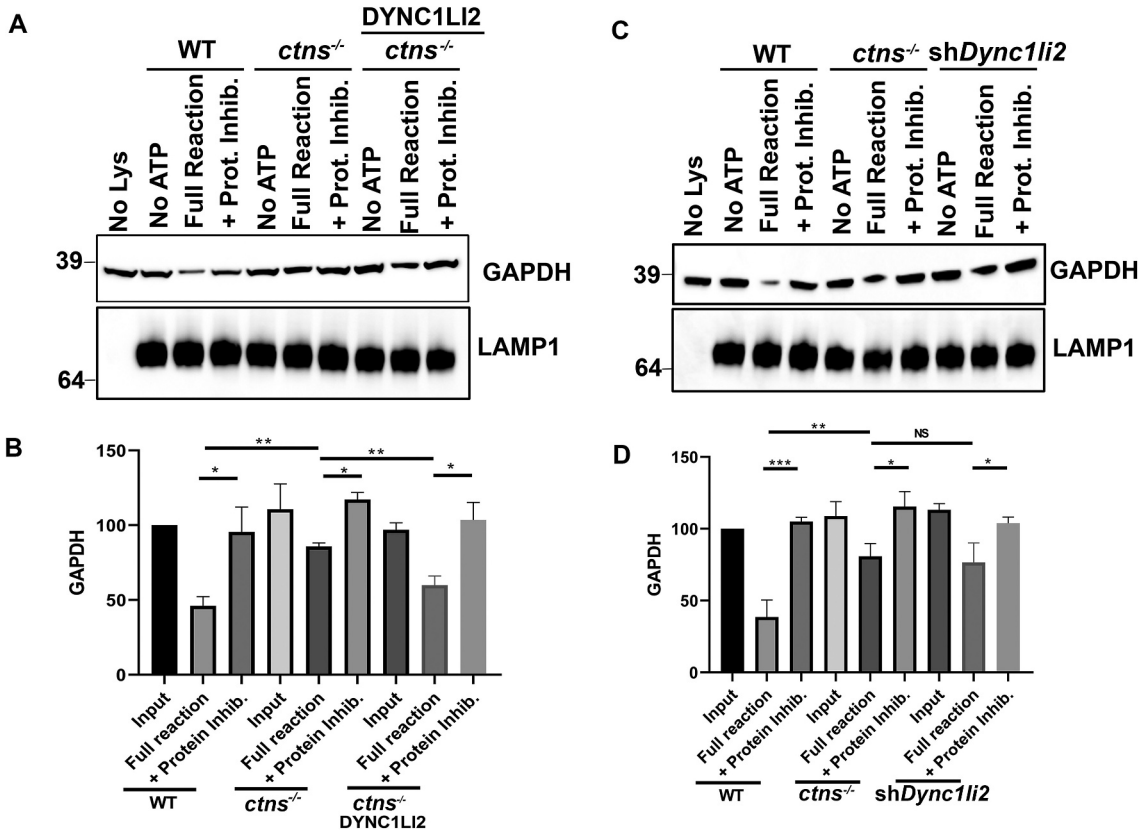

Figure 3. DYNC1LI2-downregulated cells have deficient CMA and DYNC1LI2 rescues defective CMA in cystinosis. CMA activity in isolated lysosomes analyzed by *in vitro* substrate internalization and degradation. The integrity and purity of the isolated lysosomal fractions is shown in associated Figure S2. Lysosomes isolated from WT, *ctns*$^{-/-}$, and DYNC1L2-reconstituted *ctns*$^{-/-}$ cells (A and B) or *Dync1li2*-downregulated cells (sh*Dync1li2*) (C and D) were incubated at 37°C for 30 min with the CMA substrate recombinant GAPDH, in the presence or absence of ATP regeneration system (Full reaction) or protease inhibitors (Prot. Inhib.). A fraction of the CMA reactions was resolved by SDS-PAGE and GAPDH (CMA substrate) and LAMP1 (control) detected by immunoblotting. Total protein loading control is included as additional supporting data in Figure S6. (B and D) Quantitative densitometry analysis of CMA activity performed in three independent experiments. Results are Mean ± SEM. *, $p < 0.05$, **, $p < 0.01$; ***, $p < 0.001$; NS, not significant (unpaired *t*-test) .

DYNC1LI2 reconstitution but not DYNC1LI1 decreases ER stress

In cystinosis, CMA defects are associated with increased endoplasmic reticulum (ER) stress and susceptibility to oxidative stress [3,12]. To evaluate whether the rescue of DYNC1LI2 expression has a positive impact on cellular homeostasis in cystinosis, we first analyzed the effect of DYNC1LI2 reconstitution on the expression levels of the UPR target gene HSPA5, in *ctns*$^{-/-}$ fibroblasts. Immunoblotting analysis showed that DYNC1LI2 reconstitution induces a significant decreased in the expression of endogenous HSPA5 in *ctns*$^{-/-}$ fibroblasts compared to control cystinotic cells (Figure 4A,B). *Dync1li2* downregulated sh*Dync1li2* cells showed increased HSPA5 protein levels (Figure S4B) but not significant changes in *Lamp2A* mRNA expression (Figure S4C). Different from DYNC1LI2, exogenous expression of DYNC1LI1 failed to decrease ER stress levels in *ctns*$^{-/-}$ fibroblast (Figure 4C,D). To further characterized the ER stress downstream signaling pathway in *ctns*$^{-/-}$ cells and the effect of DYNC1LI2 reconstitution in cystinosis, we next analyzed the phosphorylation of EIF2A/eIF2α (eukaryotic translation initiation factor 2A), an EIF2AK3/PERK (eukaryotic translation initiation factor 2 alpha kinase 3) substrate [43]. We observed increased EIF2A phosphorylation levels in cystinosis (Figure 4E-G). We also show increased expression and nuclear localization of ATF4 (activating transcription factor 4) in cystinosis, an ER stress-driven transcription factor involved in the response to oxidative stress [44,45], which was reverted by DYNC1LI2 reconstitution (Figure 4E,H,J). The expression level of DDIT3 was also increased in cystinosis and this increment was also reverted by DYNC1LI2 reconstitution (Figure 4E,I,K), thus supporting increased ER stress in cystinosis and partial reduction of this stress observed in *ctns*$^{-/-}$ cells following reconstitution of DYNC1LI2 expression.

DYNC1LI2 decreases mitochondria fragmentation and protects cystinotic cells from oxidative stress-induced cell death

Mitochondrial fission is an important mechanism that precedes elimination of damaged mitochondrial by mitophagy [46] and mitochondrial fragmentation is induced by oxidative stress and has been associated with human disease. Mitochondrial dysfunction has long been demonstrated in many LSDs including cystinosis [47]. Here, to establish the impact of DYNC1LI2 reconstitution on mitochondrial

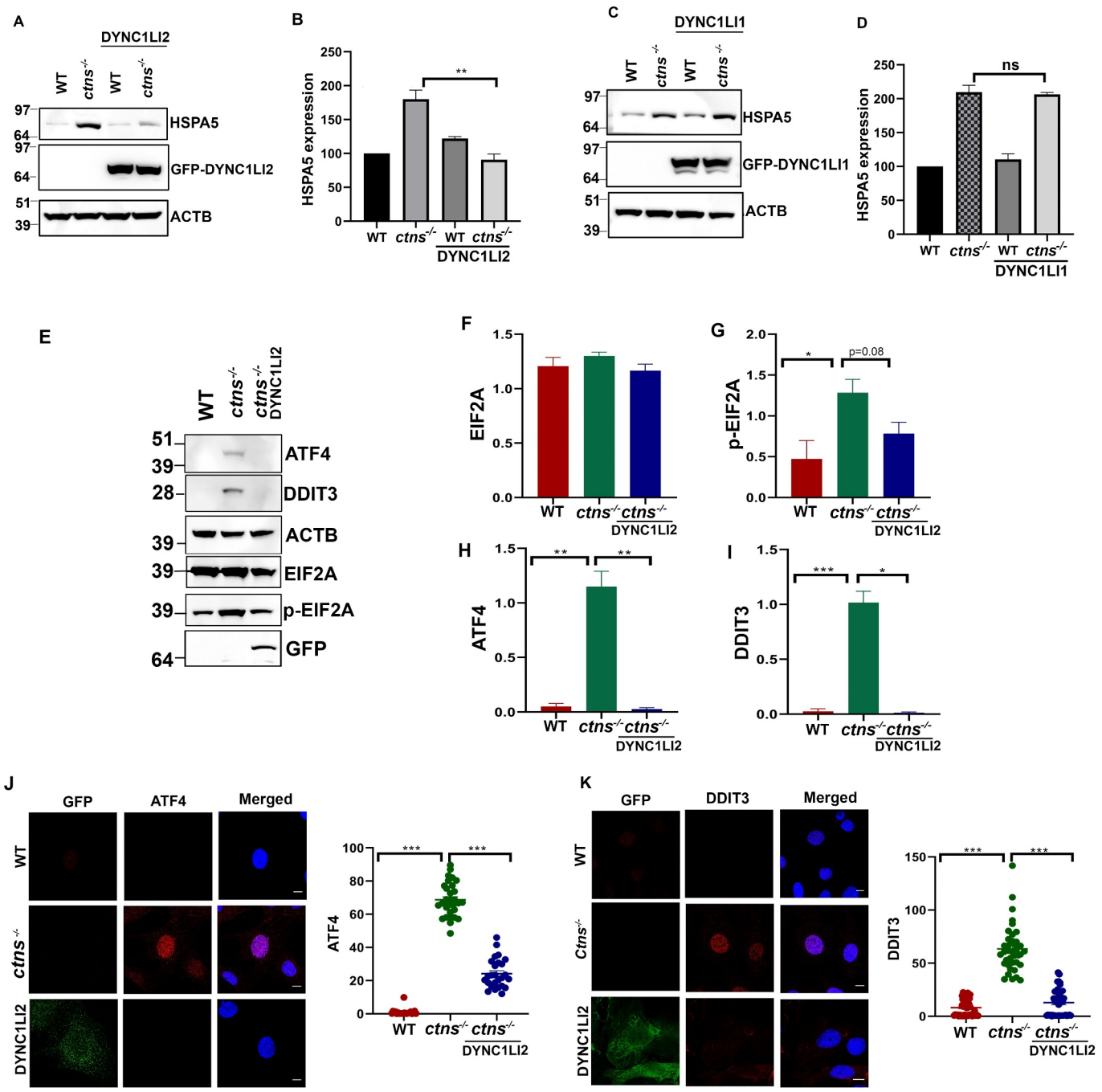

Figure 4. Rescue of DYNC1LI2 expression reduces ER stress in *ctns*$^{-/-}$ cells. (A) The expression level of the established UPR target gene HSPA5, which is induced during conditions of ER stress, was analyzed in wild-type (WT), *ctns*$^{-/-}$, and GFP-DYNC1LI2-expressing WT and *ctns*$^{-/-}$ fibroblasts by western blotting, using a mouse monoclonal anti-KDEL antibody. (B) Quantification of HSPA5 expression levels from 3 independent experiments. (C) HSPA5 expression in wild-type, *ctns*$^{-/-}$, and GFP-DYNC1LI1-expressing WT and *ctns*$^{-/-}$ fibroblasts by western blot. (D) Quantification of HSPA5 expression levels from 3 independent experiments. Mean ± SEM, **, $p < 0.01$; NS, not significant. In Figure 4A and C, HSPA5 and ACTB were detected on the same membrane. (E) Representative immunoblot analysis of the indicated ER stress markers. DDIT3 and ACTB are probed in the same membrane. Total protein loading controls for all proteins are provided in Figure S7. (F-I) Quantification of the expression of EIF2A (F), its phosphorylated form (G), ATF4 (H) and DDIT3 (I). The data is presented as Mean ± SEM from three independent experiments. (J and K) Representative images and quantitative immunofluorescence analysis of the expression of ATF4 (J) and DDIT3 (K) in WT, *ctns*$^{-/-}$, and GFP-DYNC1LI2-expressing *ctns*$^{-/-}$ cells. A total of 21 to 35 (ATF4) and 39 to 45 (DDIT3) independent images were quantified for each cell type in three independent experiments. *, $p < 0.05$; **, $p < 0.01$; ***, $p < 0.001$; NS, not significant.

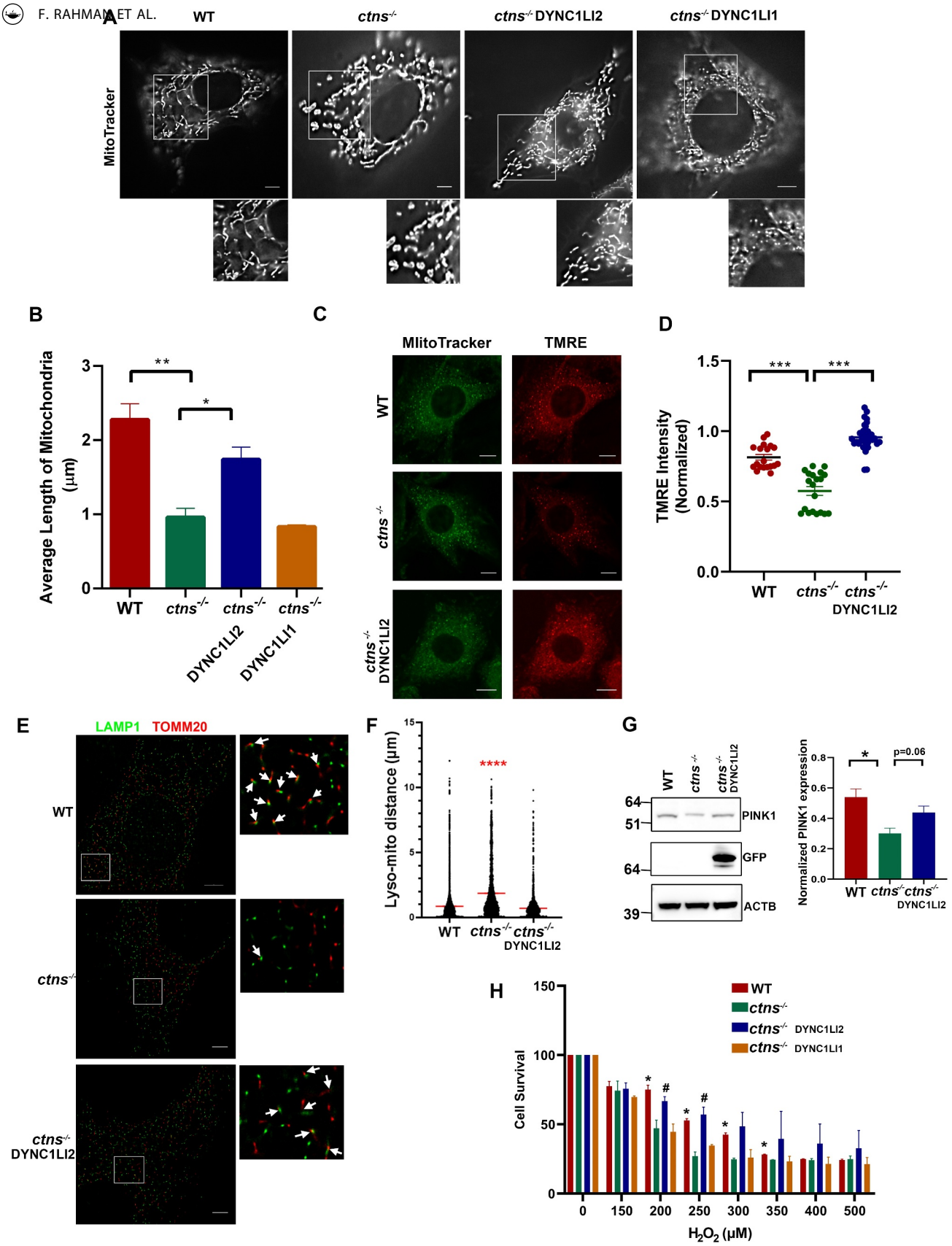

Figure 5. Reconstitution of DYNC1LI2 but not DYNC1LI1 expression decreases mitochondrial fragmentation and increases cell survival of *ctns*$^{-/-}$ cells. (A) Analysis of mitochondrial length in wild-type (WT), *ctns*$^{-/-}$, DYNC1LI2- and DYNC1LI1-expressing *ctns*$^{-/-}$ cells by pseudo-TIRFM (oblique illumination) using MitoTracker. Scale bar: 6 µm. (B) Quantification of mitochondrial length. Mean ± SEM, *, $p < 0.05$; **, $p < 0.01$ $n = 3$, 8–10 cells per experiment. (C and D) Analysis of mitochondrial membrane potential ($\Delta\psi_m$) by fluorescence microscopy. $\Delta\psi_m$ was analyzed as the ratio between the fluorescence intensity of the probe TMRE (increased fluorescence in polarized mitochondria) normalized by MitoTracker (mitochondria mass indicator). (C) Representative images. (D) Quantitative analysis from 19 to 34 WT, *ctns*$^{-/-}$, and GFP-DYNC1LI2-expressing *ctns*$^{-/-}$ cells from 3 independent experiments. (E and F) Super resolution microscopy analysis of lysosomal-mitochondrial adjacency. (E) Representative images of cells labeled with anti-LAMP1 (green) and anti-TOMM20 (pseudo-colored red). Magnified images show areas with high lysosomal-mitochondria adjacency in WT and DYNC1LI2-reconstituted *ctns*$^{-/-}$ cells (arrows) but low adjacency in *ctns*$^{-/-}$ cells. (F) Quantification of lysosomal mitochondria proximity. Pairs were plotted according to the distance to their most proximal counterpart. A total of 7202, 5778 and 4408 molecular pairs from 4 wild-type, *ctns*$^{-/-}$, and DYNC1LI2-reconstituted *ctns*$^{-/-}$ cells were analyzed by STORM. ****, $p < 0.0001$. (G) Left panel, Immunoblotting analysis of the expression of PINK1. See Figure S7 for total protein loading controls. Right panel, Quantitative analysis of PINK1 expression from 3 independent experiments. Mean ± SEM, Student's t-test. (H) GFP-DYNC1LI1 and GFP-DYNC1LI2-reconstituted MEFs were treated with H_2O_2 and cell viability was analyzed by the MTT assay. Mean ± SEM from 3 independent experiments performed in triplicates. *, $p < 0.05$, WT *vs* *ctns*$^{-/-}$; #, $p < 0.05$, *ctns*$^{-/-}$ *vs* DYNC1LI2.

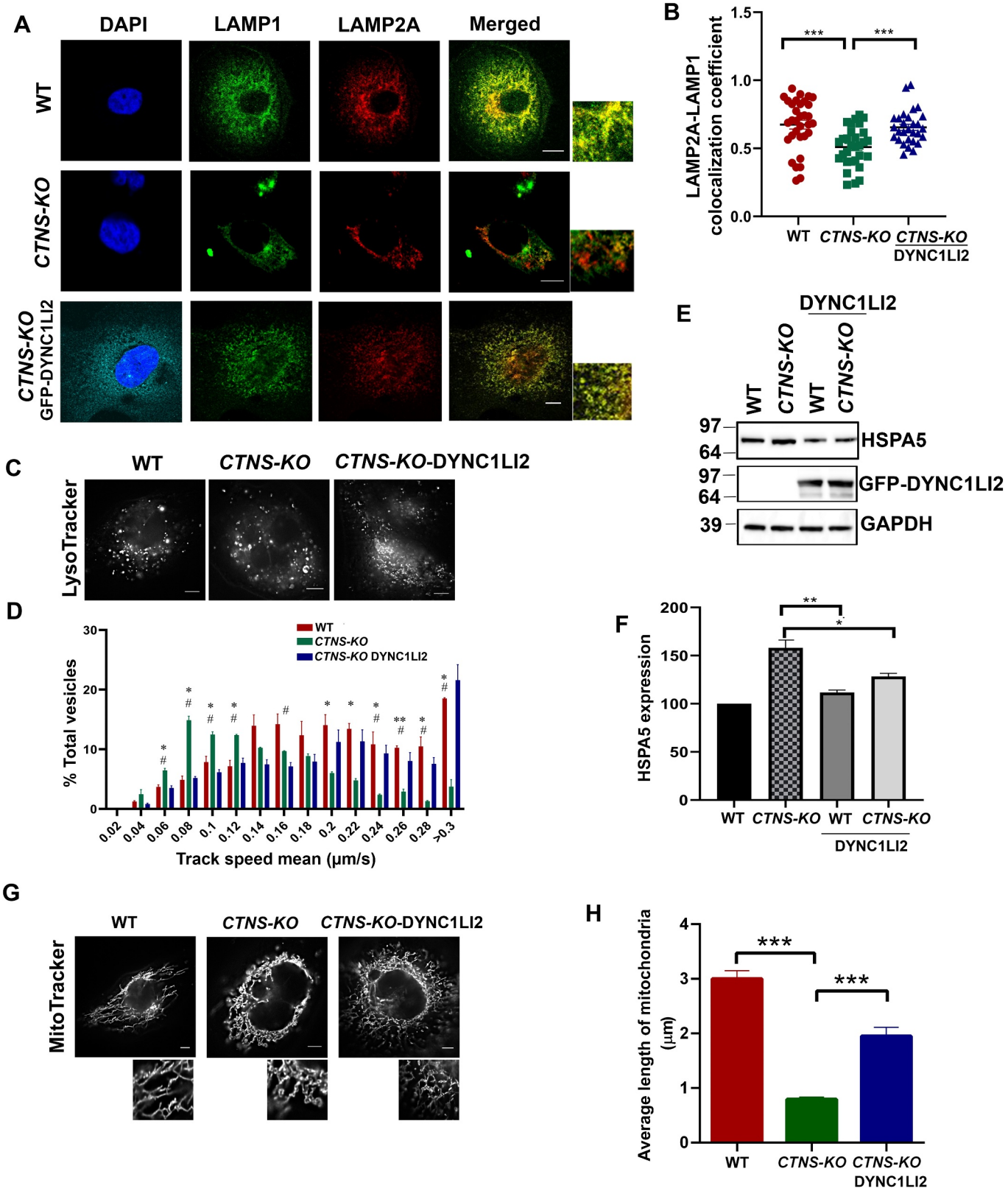

Figure 6. DYNC1LI2 rescues cellular homeostasis phenotypes in cystinotic proximal tubule cells (PTCs). (A) Immunofluorescence analysis of endogenous LAMP1 (pseudo-colored green) and LAMP2A (red) localization in wild-type, *CTNS-KO* and GFP (pseudo-colored cyan)-DYNC1LI2-expressing *CTNS*$^{-/-}$ PTCs cells. Scale bar: 10 µm. (B) Quantification of LAMP2A-LAMP1 colocalization. A total of 33, 30 and 29 fields (symbols) and 35–40 cells were quantified in each category from three independent experiments. *, p < 0.001. (C) Pseudo-TIRF microscopy analysis of PTCs labeled with LysoTracker. Scale bar: 6 µm (D) Analysis of vesicle movement of wild-type, *CTNS-KO* and DYNC1LI2 expressing *CTNS-KO* cells. The speeds for the independent vesicles were binned in 0.02 µm/s increments and plotted as a percentage of total vesicles for a given cell. Results are represented as mean ± SEM from at least 10 cells per experiments form 3 independent experiments. The statistically significant differences between the groups are indicated in the figure. Mean ± SEM, *, $p < 0.05$, **, $p < 0.01$, WT *vs* *CTNS-KO*$^{-}$ and $^{\#}$, $p < 0.05$, *CTNS-KO vs CTNS-KO* DYNC1LI2. (E) HSPA5 expression in wild-type, *CTNS-KO*, and GFP-DYNC1LI2-expressing WT and *CTNS-KO* PTCs by western blotting. (F) Quantification of HSPA5 expression from 3 independent experiments. (G) TIRF microscopy analysis of PTC labeled with MitoTracker. Scale bar: 6 µm. (H) Quantification of mitochondrial length of wild-type, *CTNS*-KO and DYNC1LI2-expressing *CTNS-KO* PTCs $n = 2$, 10–12 cells. (B, F and H), Mean ± SEM *, $p < 0.05$, **, $p < 0.01$, ***, $p < 0.001$.

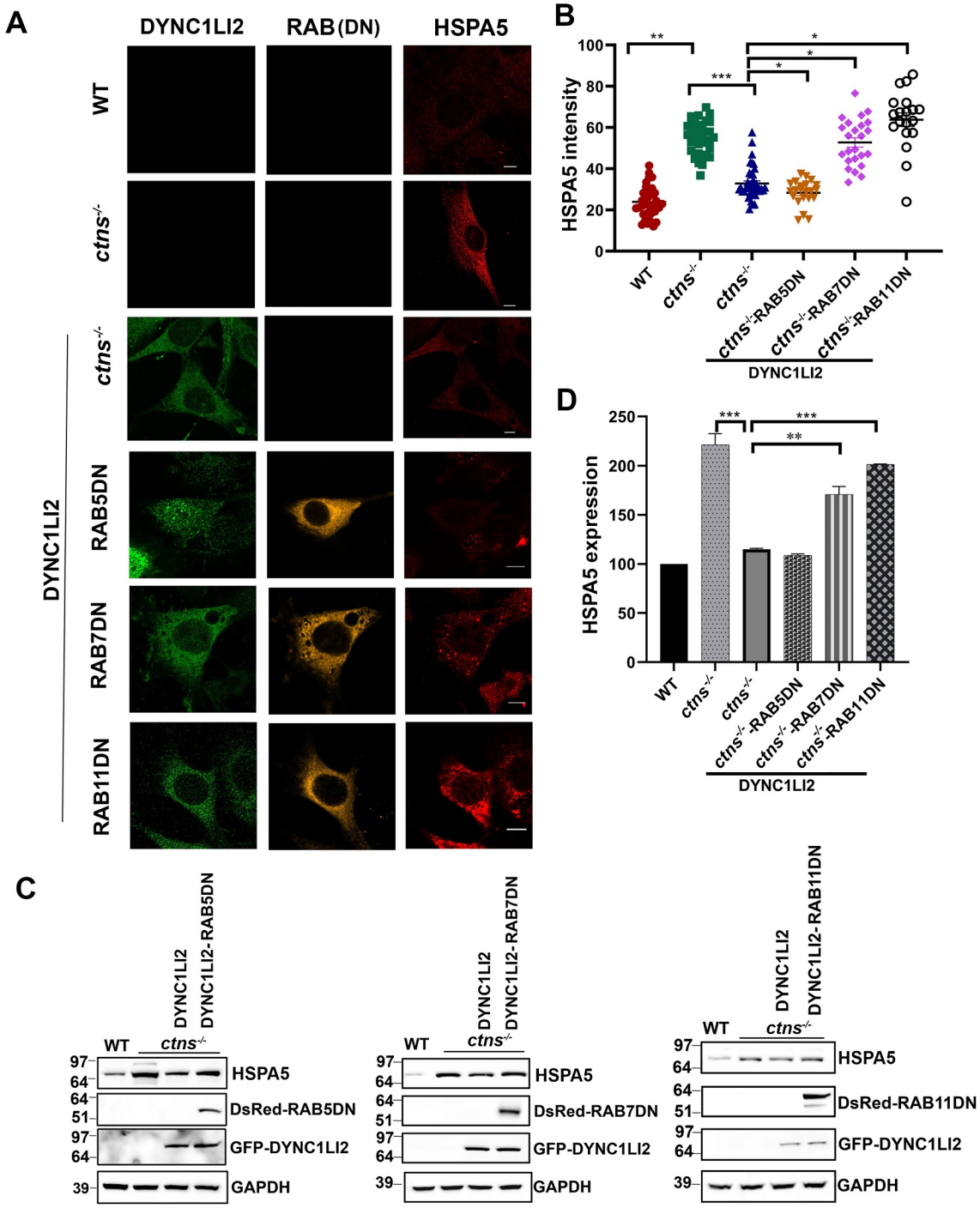

Figure 7. DYNC1LI2-dependent rescue of ER stress requires functional RAB7 and RAB11 but not RAB5. (A) Immunofluorescence analysis of the endogenous ER stress marker, HSPA5 (Red), expression in wild-type, *ctns*$^{-/-}$, *ctns*$^{-/-}$DYNC1LI2 and dominant negative (DN)-expressing RAB5DN, RAB7DN, RAB11DN, *ctns*$^{-/-}$DYNC1LI2 cells. GFP-DYNC1LI2 is shown in green. DN-RAB GTPases are pseudo-colored orange. Scale bar: 10 µm. (B) Quantification of ER stress marker expression. A total of 19–41 fields and 30–50 cells were quantified in each category, from three independent experiments. Mean ± SEM, *, $p < 0.05$, **, $p < 0.01$, ***, $p < 0.001$. (C) *Analysis of* HSPA5 expression by western blot in WT, *ctns*$^{-/-}$, *ctns*$^{-/-}$DYNC1LI2 or cells expressing DN-RABs. DsRed-RAB expression was verified by fluorescence microscopy and it is shown here by immunoblot. For detection of GFP-DYNC1LI1, GFP-DYNC1LI2 and exogenous expressed RABs the same sample mix was run in parallel and probed on separate membranes. (D) Quantification of ER stress expression levels by immunoblot from 3 independent experiments. Mean ± SEM, **, $p < 0.01$, ***, $p < 0.001$.

fragmentation in cystinotic cells, we measured mitochondria fragmentation in wild-type and *ctns*$^{-/-}$ cells expressing DYNC1LI2 or DYNC1LI1. We found that the average length of mitochondria is significantly longer in wild-type cells, reaching lengths double that of the average mitochondrial length in *ctns*$^{-/-}$ cells (Figure 5A,B). Remarkably, mitochondrial length in *ctns*$^{-/-}$ cells was significantly increased by the expression of DYNC1LI2 but not DYNC1LI1 (Figure 5B) indicating that DYNC1LI2-specific trafficking mechanisms rescue the mitochondrial morphology-defective phenotype in cystinosis. To further characterize mitochondrial function in these cells, we used TMRE to analyze

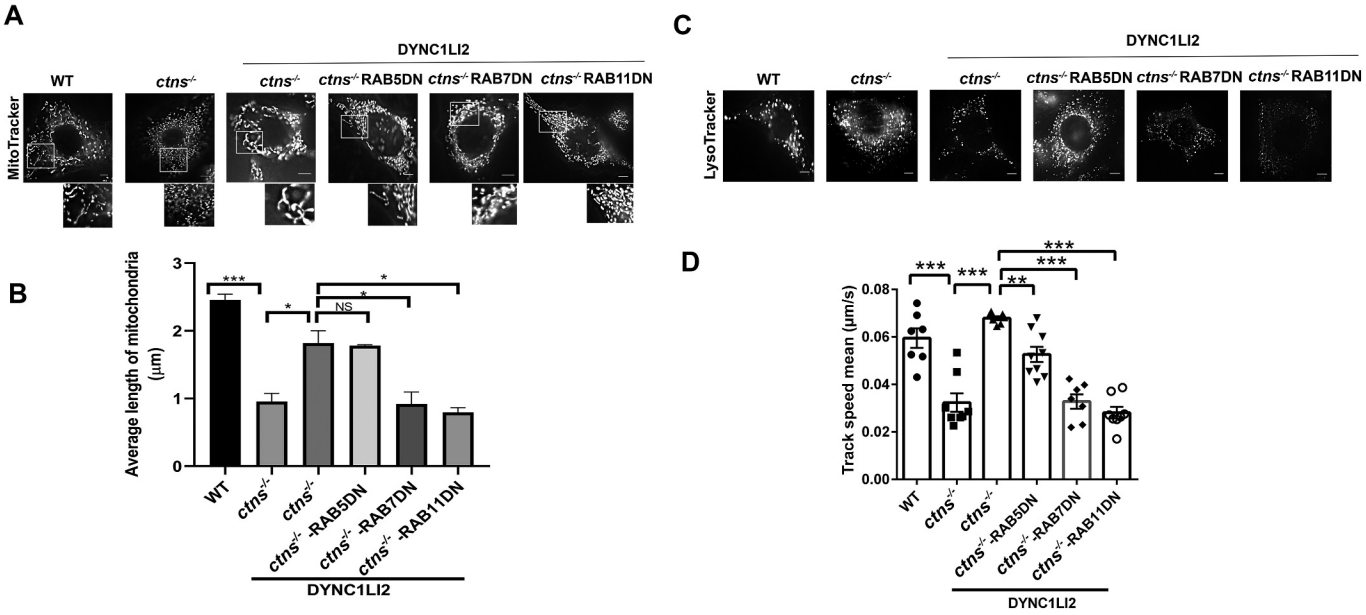

Figure 8. DYNC1LI2-mediated rescue of mitochondrial fragmentation and vesicular trafficking requires RAB7 and RAB11. (A) TIRF microscopy analysis of WT, *ctns*$^{-/-}$, *ctns*$^{-/-}$DYNC1LI2 and RAB5DN-, RAB7DN- or RAB11DN-expressing *ctns*$^{-/-}$-DYNC1LI2 fibroblasts labeled with MitoTracker. Scale bar: 6 μm. (B) Quantification of mitochondrial length. (C) Representative images of WT, *ctns*$^{-/-}$ *ctns*$^{-/-}$DYNC1LI2 and DsRed-RAB5DN-, RAB7DN-, or RAB11DN-expressing *ctns*$^{-/-}$DYNC1LI2 fibroblasts labeled with LysoTracker. Scale bar: 6 μm. (D) Analysis of vesicle movement. Results are represented as mean ± SEM from at least 7–9 cells per group. The statistically significant differences between the groups are indicated in the figure. *, $p < 0.05$, **, $p < 0.01$, ***, $p < 0.001$. NS, not significant.

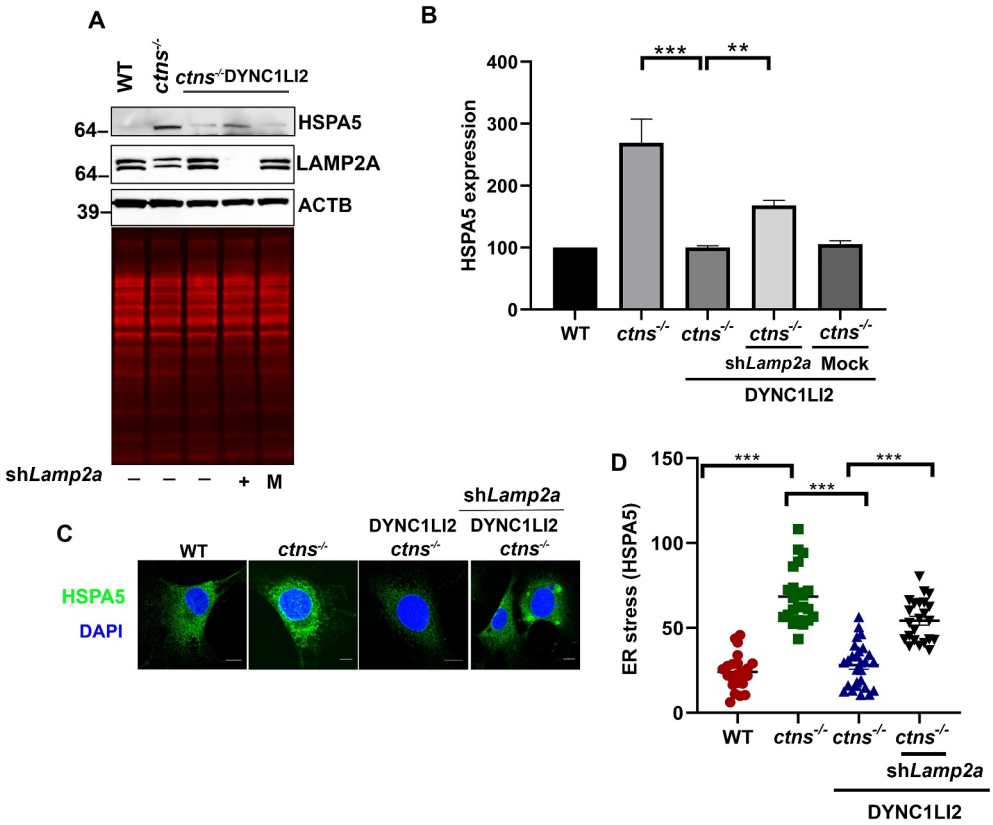

Figure 9. DYNC1LI2-mediated rescue requires the CMA receptor LAMP2A. (A) Western blot analysis of HSPA5 in WT, *ctns*$^{-/-}$, *ctns*$^{-/-}$DYNC1LI2 and LAMP2A-knockdown (sh*Lamp2a*)-expressing *ctns*$^{-/-}$DYNC1LI2 fibroblasts. M: mock infected (*ctns*$^{-/-}$DYNC1LI2- expressing stable cells infected with empty PLV-Lenti-construct). HSPA5, LAMP2A and GAPDH were analyzed in parallel; membranes are shown in Figure S8. (B) Mean ± SEM of HSPA5 expression in WT, *ctns*$^{-/-}$, *ctns*$^{-/-}$DYNC1LI2 and LAMP2A-knockdown (sh*Lamp2a*)-expressing cells. (C) Immunofluorescence analysis of endogenous ER stress marker expression in wild-type, *ctns*$^{-/-}$, *ctns*$^{-/-}$DYNC1LI2 and s sh*Lamp2a ctns*$^{-/-}$DYNC1LI2 cells. Scale bar: 10 μm. (D) Quantification of ER stress marker (HSPA5) intensity. A total of 23–27 images (symbols) for a total of 30–35 cells were quantified in each category in 3 independent experiments. Mean ± SEM, ***$p < 0.001$.

mitochondrial membrane potential, which was decreased in *ctns*$^{-/-}$ cells but elevated in DYNC1LI2-reconstituted cells (Figure 5C,D). This correlated with altered mitochondrial-endolysosomal proximity measured by super-resolution microscopy analysis of the localization of TOMM20 (translocase of outer mitochondrial membrane 20) and LAMP1 at the nanometer level using STORM. In this assay, we found decreased lysosomal-mitochondria association in cystinotic cells, which supports that removal of damaged mitochondria by lysosomes might be impaired in cystinosis (Figure 5E,F). This correlated with decreased expression levels of PINK1 (PTEN induced kinase 1) in cystinotic cells, a protein associated with clearing depolarized mitochondria by mitophagy [48], which was partially increased by DYNC1LI2 rescue (Figure 5G).

Because mitochondrial dynamics have direct impact on cell death [49] and impaired CMA leads to increased susceptibility to oxidative stress-induced cell death in cystinotic cells [3] while CMA upregulation increases survival, we next analyzed the effect of DYNC1LI2 on cell survival to pro-oxidant insults. We show that *ctns*$^{-/-}$ cells have increased endogenous levels of reactive oxygen species determined using the ROS-sensitive fluorescent probe CellROX™ and that DYNC1LI2 reconstitution decreases ROS in these cells (Figure S5). To analyze cell survival to exogenous oxidative stress, wild-type, and *ctns*$^{-/-}$ cells expressing either DYNC1LI2 or DYNC1LI1 were exposed to increasing concentrations of H_2O_2 and the cellular metabolic activity was analyzed by the MTT assay as an indication of cell survival. *ctns*$^{-/-}$ cells showed increased susceptibility to oxidative stress-induced cell death compared to wild-type cells, shown here, in Figure 5H, and before in Ref [11]. Notably, the expression of DYNC1LI2 was protective, significantly increasing the survival of *ctns*$^{-/-}$ cells (Figure 5H) and this positive effect was not observed in cells expressing the paralog light intermediate subunit, DYNC1LI1.

DYNC1LI2 corrects the cellular homeostasis-defective phenotypes of cystinotic proximal tubule cells

Proximal tubular cells (PTCs) are the most affected cells in nephropathic cystinosis and PTC dedifferentiation contributes to the development of Fanconi syndrome [50]. Similar to fibroblasts, cystinotic PTCs have decreased DYNC1LI2 expression (Figure 1), LAMP2A mislocalization, defective CMA and impaired vesicular trafficking [11,39]. Furthermore, *CTNS*-KO cells are characterized by increased HSPA5 expression and ER stress and decreased expression of the RAB-GTPase RAB11, a carrier of the chaperone-mediated autophagy receptor LAMP2A and a regulator of LRP2/megalin trafficking to the apical membrane [11,39]. To study the possible beneficial impact of DYNC1LI2 expression reconstitution in PTC function, we next analyzed the localization of the CMA receptor LAMP2A in DYNC1LI2-expressing cystinotic PTCs (*CTNS*-KO) which were developed using CRISPR-*Cas*9 technology [39]. We found that DYNC1LI2 reconstitution rescues LAMP2A localization at lysosomes in *CTNS*-KO cells (Figure 6A,B). Furthermore, DYNC1LI2 corrected vesicular trafficking (Figure 6C,D), in particular, DYNC1LI2 recovered the dynamic behavior of a subpopulation of highly motile vesicles, those moving at >0.2 μm/sec, which were previously associated with RAB7-dependent movement [11]. In addition, DYNC1LI2 decreased ER stress levels (Figure 6E,F) and partially corrected the mitochondria hyperfragmentation phenotype in cystinotic PTCs (Figure 6G,H).

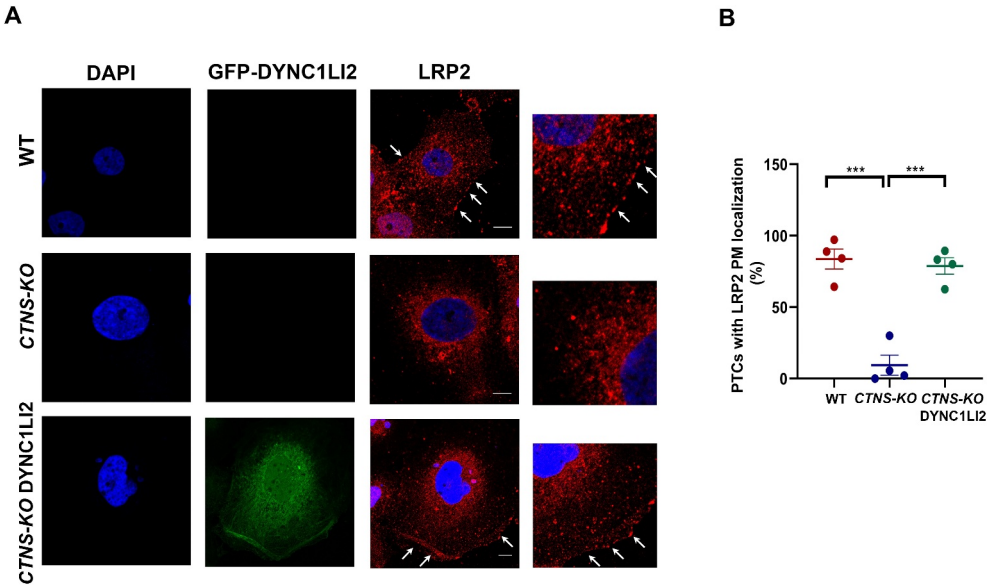

Figure 10. DYNC1LI2 increases LRP2 localization at the plasma membrane in cystinotic proximal tubule cells. (A) Immunofluorescence analysis of LRP2/megalin localization in wild type, *CTNS*$^{-/-}$ (KO) and GFP-DYNC1LI2 expressing *CTNS*$^{-/-}$ proximal tubule cells (B) Quantitative analysis of LRP2 localization. A total of 15 to 35 cells were quantified per group in each experiment. The data correspond to 4 independent experiments. Each symbol indicates the mean for each experiment and bars indicate the SEM. ***, $p < 0.001$.

DYNC1LI2-mediated rescue of cystinotic cell function requires both RAB11 and RAB7 but not RAB5

DYNC1LI1 and DYNC1LI2 function as linkers between the motor subunit and the transported organelle through interactions with multiple regulatory molecules [18,33]. Two of these molecules, RILP and RAB11FIP3, are specific effectors of the small RAB GTPases RAB7 and RAB11, which are also known to regulate late and recycling endosomal trafficking, respectively. Coincidently these GTPases mediate LAMP2A trafficking and are therefore important regulators of CMA [11]. Although both DYNC1LI1 and DYNC1LI2 are described to bind to RILP and RAB11FIP3, differential regulation of these interactions by PKA-mediated phosphorylation led to the suggestion that DYNC1LI2 regulates a subpopulation of dynein-associated endolysosomes different from that regulated by DYNC1LI1 [40].

To analyze whether the rescue mediated by DYNC1LI2 requires RAB GTPases of the endocytic pathways, we analyzed homeostatic mechanisms in cystinotic cells reconstituted with DYNC1LI2 and expressing dominant-negative (DN) RAB5, RAB7 or RAB11 GTPases, mutants that are only present in the GDP-bound form and are therefore unable to bind to their specific effectors. The cells were utilized in ER stress analysis by two independent approaches. First, we performed immunofluorescence analysis of endogenous KDEL-positive ER chaperones (Figure 7A,B). Second, we analyzed the expression level of HSPA5 by immunoblot (Figure 7C,D). In both assays, we show that DN-RAB7 and DN-RAB11 but not DN-RAB5 preclude the rescue of the phenotype mediated by DYNC1LI2. Thus, using two independent assays, we found that the rescue of the increased ER stress phenotype mediated by DYNC1LI2 requires both functional RAB7 and RAB11 but not RAB5 GTPases.

Next, we studied whether functional RAB GTPases were necessary for DYNC1LI2 to rescue mitochondrial fragmentation and vesicular trafficking. To this end, we first analyzed mitochondrial morphology in RAB5 dominant negative (DN), RAB7DN or RAB11DN-expressing *ctns*$^{-/-}$ cells reconstituted with DYNC1LI2. We found that DYNC1LI2 was able to rescue mitochondrial dynamics when co-expressed with RAB5DN but not when RAB7DN or RAB11DN were co-expressed in these cells (Figure 8A,B). Also, the upregulation of DYNC1LI2 in *ctns*$^{-/-}$ cells failed to reestablish normal endolysosomal dynamics when co-expressed with nonfunctional endolysosomal RABs, RAB7DN and RAB11DN, (Figure 8C,D). RAB5DN only weakly interfered with DYNC1LI2-mediated trafficking upregulation, thus establishing RAB7 and RAB11 as the main effectors of DYNC1LI2-mediated upregulation of vesicular trafficking in cystinosis.

DYNC1LI2-mediated rescue of cystinotic cell function requires the CMA receptor LAMP2A

Trafficking and lysosomal localization of the CMA receptor LAMP2A is mediated by RAB7, its effector RILP, and RAB11 [11]. CMA activators increase vesicular trafficking and mediate RAB11 upregulation but LAMP2A knockdown prevents the improvement of cell survival mediated by CMA activators [39]. Here, we analyzed whether DYNC1LI2-dependent rescue of the cystinotic defective phenotype was dependent on LAMP2A. To this end, we analyzed ER stress in cystinotic cells reconstituted with DYNC1LI2, in which LAMP2A expression was downregulated using specific, and previously validated [11], lentiviral LAMP2A-shRNAs. In Figure 9A,B, we show that the rescue mediated by DYNC1LI2 reconstitution is significantly impaired in cells with decreased expression levels of the CMA receptor LAMP2A. In an independent approach, we analyzed the effect of LAMP2A-downregulation on KDEL expression in cystinotic cells reconstituted with DYNC1LI2 using immunofluorescence analysis of endogenous ER chaperones (Figure 9C,D). Again, LAMP2A downregulation blocked the ability of DYNC1LI2 to rescue the defective phenotype in cystinosis, thus supporting that LAMP2A and CMA function are necessary for DYNC1LI2 to correct cell function in cystinosis.

DYNC1LI2 increases LRP2 localization at the plasma membrane in cystinotic proximal tubule cells

The loss of apical receptors, including LRP2, leads to PTC dedifferentiation in cystinosis. The recycling of LRP2 to the plasma membrane is regulated by RAB11, whose expression is downregulated in cystinosis. Upregulation of RAB11 rescues LAMP2A lysosomal localization in these cells. Here, we next analyze whether DYNC1LI2 expression reconstitution positively impacts endocytic receptor distribution in cystinotic PTCs. To this end, we analyzed the localization of the apical receptor LRP2 in wild-type, *ctns*$^{-/-}$ cells and cells with reconstituted expression of DYNC1LI2. Remarkably, DYNC1LI2 significantly increased the plasma membrane localization of LRP2 in cystinotic PTCs (Figure 10A,B) suggesting that DYNC1LI2 upregulation has the potential to improve tubular cell function in cystinosis.

Discussion

Impaired vesicular trafficking leads to defects in the maintenance of cellular homeostasis but the molecular mechanisms mediating these processes are not well-understood. The HSPA8-dependent translocation of proteins destined for degradation in the lysosome by a process referred to as chaperone-mediated autophagy (CMA), requires the presence of LAMP2A, the only known receptor for CMA, at the lysosomal membrane [34]. Efficient translocation of LAMP2A to the lysosome requires the small GTPases RAB7 and RAB11 [11]. The dysregulation of this mechanism is particularly manifested in the lysosomal storage disease cystinosis, in which LAMP2A is retained at RAB11-positive carrier vesicles with the deleterious effect that the consequent impairment in CMA decreases cell survival [3]. Here, we show that the vesicular trafficking regulator, DYNC1LI2, is downregulated in cystinosis, and its reconstitution corrects the impaired cellular homeostasis by decreasing ER stress and mitochondrial fragmentation. Thus, DYNC1LI2 emerges as a molecular target

whose upregulation may improve cellular function in this lysosomal storage disorder.

Because only a subpopulation of lysosomes is active for CMA, LAMP2A lysosomal localization and stabilization at the lysosomal membrane are essential mechanisms to maintain cellular homeostasis. Furthermore, activation of CMA induces the relocalization of CMA-competent lysosomes from the cell periphery to the perinuclear area [51]. In this context, the finding that DYNC1LI2, a protein involved in retrograde transport, regulates LAMP2A lysosomal localization and CMA mediated functions, has important biological significance. Our data showing that DYNC1LI2-mediated rescue of the defective phenotypes observed in cystinosis is attenuated in LAMP2A-downregulated cells establishes a direct link between vesicular trafficking, CMA and cellular homeostasis.

Several RAB GTPases and their effectors have been described to act as molecular links between the dynein molecular machinery and the cargoes they transport. For example, the sorting endosome GTPase, RAB4A, has been implicated in the localization of endosomes to microtubules through the direct binding to DYNC1LI1 in a GTP-dependent manner [24]. The small GTPase RAB11 and its effector RAB11FIP3 were later shown to regulate the endosomal-recycling compartment through binding to both intermediate-light chains, DYNC1LI1 and DYNC1LI2 [31,32]. The RAB7 effector RILP was originally associated with DCTN1/dynactin p150^{Glued}, a mechanism that regulates the recruitment of late endosomes to the dynein motor [52]. Later, RILP was shown to recruit late endosomes to dynein motor-associated microtubules through DYNC1LI1 in a dynactin-independent manner [30]. Although downregulation of either DYNC1LI1 or DYNC1LI2 was shown to affect late endosome distribution, based on the more clear association of DYNC1LI1 to late endosomes, it was proposed that DYNC1LI1 plays a more critical role in the endocytic pathway [30]. Here, we show that inactivation of either RAB11 or RAB7 was sufficient to prevent the rescue of cellular homeostatic mechanisms mediated by DYNC1LI2, thus functionally linking DYNC1LI2 to these GTPases. In principle, this suggest that DYNC1LI2 operates through RAB11 and RAB7 by two essential and independent trafficking mechanisms. While interference with either RAB7 or RAB11 affects the trafficking kinetic parameters of LAMP2A, only RAB7 interference affects the movement of a fast-moving subcellular pool of LAMP2A-positive vesicles [11]. Together, these data suggest that LAMP2A may require the regulation of two sequential mechanisms mediated by RAB11 and RAB7, and that DYNC1LI2 may facilitate this transition. The observation that DYNC1LI2 preferentially upregulates the dynamics of highly motile endo-lysosomes, RAB7-expressing vesicles, further support this hypothesis. Alternatively, RAB7 and RAB11 may define two independent sub-types of LAMP2A-positive vesicles but both pools should be necessary to translocate competent amounts of LAMP2A to lysosomal membranes.

Both DYNC1LI1 and DYNC1LI2 bind to the dynein motor heavy chain as well as to RAB11 and RAB7 effectors. However, only DYNC1LI2 but not DYNC1LI1 is downregulated in cystinosis and expression of DYNC1LI2 but not DYNC1LI1 rescued the defective phenotypes observed in cystinotic cells. This suggests that specific molecular determinants in addition to motor subunits and RAB adaptors are necessary for DYNC1LI2 to specifically exert its biological function in cystinotic cells. Of note, the interaction of DYNC1LI1 but not DYNC1LI2 with RAB effectors is regulated by post-translational modification including phosphorylation [40] and so, it is possible that this type of regulation is absent in cells where DYNC1LI2 is predominantly active.

In conclusion, we show that DYNC1LI2 but not DYNC1LI1 plays a fundamental role in the translocation of LAMP2A to CMA-competent lysosomes and identified LAMP2A and CMA as a novel mechanism modulated by DYNC1LI2. This mechanism is directly associated with the maintenance of important cellular homeostatic processes in a RAB7- and RAB11-dependent manner. Thus, DYNC1LI2 upregulation leads to the correction of defective phenotypes including endoplasmic reticulum stress, increased mitochondria fragmentation and decreased cell survival. These conditions are particularly manifested in cystinotic cells, thus highlighting a role for DYNC1LI2 in vesicular trafficking in this disease. Because upregulation of DYNC1LI2 leads to the correction of cellular homeostatic mechanisms and increases the expression the endocytic receptor LRP2 at the plasma membrane of cystinotic proximal tubule cells, DYNC1LI2 emerges as a new possible target to correct pathological processes specific for kidney dysfunction in this lysosomal storage disorder.

Materials and methods

Animal models and cell lines

All animal studies were performed in compliance with the United States Department of Health and Human Services Guide for the Care and Use of Laboratory Animals. All studies were conducted according to National Institutes of Health and institutional guidelines and with approval of the animal review boards at The Scripps Research Institute and University of California, San Diego. The C57BL/6 *ctns*$^{-/-}$ mice were described previously [53]. Neonatal mouse embryonic fibroblasts from *ctns*$^{-/-}$ and wild-type mice were prepared by standard procedures [3]. The cystinosin knockout human proximal tubule cell line was generated using CRISPR-Cas9 and described previously [39]. Neonatal murine fibroblasts, proximal tubule cell line and 293 FT cells (ATCC, CRL-3216) were maintained in Dulbecco's modified Eagle's medium (Gibco, 11,965–092) supplemented with 10% FBS (Corning Cellgro, 10,082–147) and penicillin-streptomycin-glutamine (Life Sciences, 10,378–016).

Gene expression microarray analysis

Animals were housed and studied according to NIH Guidelines for the Care and Use of Laboratory Animals. Sixteen months old C57BL/6 wild-type (n = 6) and *ctns*$^{-/-}$ (n = 6) mice were euthanized, and the kidneys immediately removed and stored at -80°C in RNA Later (Invitrogen, AM7024). Tissues were subsequently ground using Precellys 24 (Bertin Technologies, P000669-PR240-A) and RNA was

isolated using the Qiagen AllPrep DNA/RNA Mini kit (Qiagen, 74,104). The RNA was run on a Bioanalyzer (Agilent) for quantification and quality assessment. The Ambion WT Expression Kit was used to generate double-stranded biotinylated cDNA and the Affymetrix HT WT Terminal Labeling Kit was used to prepare the cDNA for hybridization to Affymetrix GeneChip Mouse Gene 1.1 ST arrays. The double-stranded biotinylated cDNA from each tissue for each mouse was run on individual Affymetrix GeneChip. The data was collected as CEL files and quality control analysis performed with Affymetrix Expression Console. Normalized signal intensities were generated with Robust Multichip Average (RMA) which employs a background adjustment and quantile normalization strategy [54]. Genes without an average $\log_2$ transformed signal above 6 in either the wild-type or *ctns*$^{-/-}$group were removed from further analysis. Class comparisons of variance by two-way t-tests for two sample comparisons ($p < 0.001$) were performed using BRB-ArrayTools (http://linus.nci.nih.gov/BRB-ArrayTools.html) to identify the set of significantly differentially expressed genes between wild-type and *ctns*$^{-/-}$ mice in each tissue. Pathway analyses were performed, and images generated using ROSALIND™, OnRamp BioInformatics.

Constructs, transfections, and transductions

Lentiviral vectors expressing pLVXGFP-DYNC1LI2 (66,601), pLVXGFP-DYNC1LI1 (66,600), were obtained from Addgene (deposited by Dr. David Stephens) and were analyzed by sequencing for confirmation (Retrogene). The pLVGFP (Gift, S. Cherqui, UCSD) expression vector was used as a control in mock infections. 293 FT cells were transfected with the pLV constructs along with packaging plasmids pVSVG (Addgene, 8454; deposited by Dr. Robert A Weinberg) and pLV-CMV-delta 8.2 (Addgene, 12,263; deposited by Dr. Didier Trono) using the Lipofectamine LTX transfection reagent (Thermo Fisher Scientific, 2,103,388). Virus-containing supernatants were collected at 24 and 48 h post transfection, filtered, and then used to infect cells without additional processing or concentration. Wild-type and *ctns*$^{-/-}$ type cells of murine fibroblasts and PTC cells were transduced with lentiviruses in the presence of 5 μg/ml Polybrene (Millipore-Sigma, TR-1003-G). After 24 h, the virus-containing medium was replaced with normal growth medium. The transduction efficiency obtained using this procedure was > 90% [12]. To make stable cell lines, infected cells were kept under selection pressure for puromycin (100,552, MP Biomedicals, LLC), selected by GFP-expression and analyzed by WB to select cells that maintained stable levels of expression. The constructs DsRed-RAB5DN (Addgene, 35,139; deposited by Dr. Sergio Grinstein), DsRed-RAB7DN (Addgene, 12,662; deposited by Dr. Richard Pagano) were described previously [11]. Expression vectors for the expression of DsRed-RAB11DN (12,680; deposited by Dr. Richard Pagano) was purchased from Addgene [11,55]. DYNC1LI2 expressing *ctns*$^{-/-}$ MEF cells and 293 FT cells were transfected using Lipofectamine 3000 (Thermo Fisher Scientific, 2,103,388) following the manufacturer's instructions. Lentiviral mouse *Lamp2a* shRNA (Gift, Dr. A.M. Cuervo, Albert Eisntein College of Medicine) was transduced in DYNC1LI2-*ctns*$^{-/-}$ cells also as described before [11]. Lentiviral mouse mcherry-sh*Dync1li2* (MSH097725-LVRU6MP-a) and mock mCherry-shRNA (CSHCTR001-I-LVRU6MP) were from Genecopeia.

Gel electrophoresis and immunoblotting

Cells were lysed in lysis buffer (20 mM Tris, pH 7.4, 150 mM NaCl, and 1% Triton X-100 [Fisher Scientific, BP151-500]) in the presence of protease inhibitors (Roche Applied Science, 30,496,700) and phosphatase inhibitors (Calbiochem, 524,624 and 524,625). Protein concentration in diluted samples (0.01% Triton X-100) was measured using the colorimetric Bradford assay (Bio-Rad, 5,000,006). Gel electrophoresis was carried out using 4–12% gradient or 12% Bolt Bis-Tris Plus gels (Life Technologies, NW00122BOX). Proteins were transferred onto 0.45-μm nitrocellulose membranes (GVS Filter Technology, 1,215,484) and the membranes were incubated overnight at 4°C in the indicated primary antibodies, followed by incubation with HRP-conjugated secondary antibodies (Bio-Rad Laboratories, goat anti-mouse HRP, 170–6516; or goat anti-rabbit HRP, 170–6515). The blots were developed using SuperSignal West Pico (Thermo scientific, 34,580), clarity ECL Western blotting substrate (Bio-Rrad, 1,709,060) or Femto chemiluminescence substrate systems (Thermo Fisher Scientific, 34,094). Proteins were visualized using Azure Biosystems C600 technology. Total loading was detected using Revert 700 Total Protein Stain (VWR, 103,546–314) or Ponceau S staining reagent (Sigma, P3504), in addition to housekeeping genes, to control for equal loading. Uncropped blots and total protein loading controls are shown in Figures S6-S8. All gels included 15 μg of total protein per lane. Standard curves showed linearity of the ACTB signal up to at least 20 μg of lysate protein per lane (Figure S9). The C600 utilizes CCD detectors that register signals in a range of 2^{16} = 65,536 shades in grayscale, which indicates the instruments detect 4.82 orders of magnitude, a very wide dynamic range that allows for very strong and weak bands to be detected with a background contribution that tends to be negligible. Images are presented as acquired without any brightness or contrast adjustments. GFP-DYNC1LI1 and GFP-DYNC1LI2 expressing cells are stable cell lines. Despite their expression levels being constant in time, GFP-DYNC1LI1 and GFP-DYNC1LI2 expression is presented in all blots. Because GFP-DYNC1LI1 and GFP-DYNC1LI2 have similar electrophoresis migration behavior as HSPA5, for the detection of GFP-DYNC1LI1 and GFP-DYNC1LI2 the same sample mix was run in parallel and GFP-DYNs were detected on separate membranes. The following antibodies were used for immunoblotting in this study: rabbit anti-DYNC1LI2 (ThermoFisher Scientific, PA5-45,861), anti-DYNC1LI1 (ThermoFisher Scientific, PA5-31,644), anti-RAB5 (Cell Signaling Technology, 2143 T), anti-RAB7 (Cell Signaling Technology, 9367S), anti-RAB11A (Cell Signaling

Technology, 5589S), anti-ACTB/beta actin (Santa Cruz Biotechnology, sc-7210 or sc-47,778); anti-GAPDH (GeneTex, GT239); anti-GFP (Santa Cruz Biotechnology, SC-9996), anti-FLAG (Genecopoeia, CGAB-DDK-0050) and anti-KDEL (Enzo Life Sciences, ADI-SPA-827), anti-LAMP1 (Santa Cruz Biotechnology, sc-19,992); anti-LAMP2A (ThermoFisher Scientific, 51–2200), Anti-TOMM20-D8T4N (Cell Signaling Technology, 42406S), anti-mCherry (Rockland Immunochemicals, Inc., 600–401-P16), anti-PINK1 (ThermoFisher Scientific, PA5-85,930), anti-EIF2A /elF2α (Cell Signaling Technology, 9722S), anti-phospho-EIF2A/elF2α (Cell Signaling Technology, 3398S), anti-ATF4 (Cell Signaling Technology, 11815S), and anti-DDIT3/CHOP (Cell Signaling Technology, 2895S). The dilution of the antibodies used for immunoblotting is indicated in "antibody list" in Table S2.

Immunofluorescence, immunohistochemistry, and confocal analysis

Murine fibroblast and PTCs were seeded at 70% confluence in a 4-chamber 35-mm glass-bottom dish (In Vitro Scientific, D35 C4-20-1.5-N), then fixed with 4% paraformaldehyde (Electron Microscopy Sciences, 15,710,) for 8 min and blocked with 1% BSA (Rockland, BSA-50) in PBS (Corning, 21–031-CV), in the presence of 0.01% saponin (Calbiochem, 558,255), for 1 h. Samples were labeled with the indicated primary antibodies overnight at 4°C in the presence of 0.01% saponin and 1% BSA. Samples were washed 3 times and subsequently incubated with the appropriate combinations of Alexa Fluor (488 or 594)-conjugated anti-rabbit, anti-rat, or anti-mouse secondary antibodies (Thermo Fisher Scientific, A-21206; A-21207; A-21208; A-21209; A-21202; A-21203, respectively). Nuclei were stained with 4,6-diamidino-2 phenylindole (DAPI; Millipore-Sigma, D9542) and samples were preserved in Fluoromount-G reagent (SouthernBiotech, 0100–01) and kept at 4°C until analyzed. Samples were analyzed with a Zeiss LSM 710 or Zeiss LSM 880 laser-scanning confocal microscope attached to a Zeiss Observer Z1 microscope at 21°C, using a 63x oil Plan Apo, 1.4-numerical aperture objective. Images were collected using ZEN-LSM software and processed using ImageJ and Adobe Photoshop CS4. The exposure time and gain were maintained throughout the experiment to comparatively analyze wild-type and *ctns*$^{-/-}$ cells. Analysis and quantification of protein colocalization were performed using ZEN-LSM software. The following antibodies were used for immunofluorescence in this study: anti-LAMP1 (Santa Cruz Biotechnology, sc-19,992); anti-LAMP2A (Abcam, ab18528 or Thermo Fisher Scientific, 51–2200); rabbit anti-GFP (Novus Biologicals, NB600-308SS) and anti-KDEL (Enzo Life Sciences, ADI-SPA -827); anti-LRP2 (Santa Cruz, sc-16,476). Anti-TOMM20-D8T4N (Cell Signaling Technology, 42406S), anti-ATF4 (Cell Signaling Technology, 11815S), anti-DDIT3 (Cell Signaling Technology, 2895S).

TIRF microscopy

Cells labeled with LysoTracker (Invitrogen, L7528) and MitoTracker (Cell Signaling Technology, 8778) were transferred to a microscope stage and maintained at 37°C. Pseudo-TIRF microscopy (oblique illumination) experiments were performed using a X100 1.45 numerical aperture TIRF objective (Nikon) on a Nikon TE2000U microscope custom-modified with a TIRF illumination module as described [11]. Images were acquired on a 14-bit cooled charge-coupled device camera (Hamamatsu) controlled through NIS-Elements software. For live cell imaging, the images were recorded using 200–500-ms exposures depending on the fluorescence intensity of the sample. The track speed mean was then analyzed using Imaris as described before [11,39]. Wild-type and *ctns*$^{-/-}$ cells were analyzed comparatively by maintaining exposure time and gain throughout the experiment. Length of mitochondria were analyzed using the "Measure" tool in ImageJ software.

Super-resolution microscopy (STORM) analysis of mitochondrial-lysosomal association

Cells were fixed in 4% PFA, blocked in 3% BSA, 5% goat serum (MP Biomedicals, 64,292), 0.01% saponin in PBS and stained with rabbit anti-TOMM20 antibody and rat anti-LAMP1 antibody followed by Alexa Fluor 488 conjugated donkey anti-rat and Alexa Fluor 647 conjugated donkey anti-rabbit secondary antibodies, respectively. After staining, samples were post-fixed with 4% PFA, placed in STORM buffer (50 mM Tris, pH 8.0, 10 mM NaCl, 10% glucose, 0.1 M mercaptoethanolamine [Sigma, M3148], 56 units/ml glucose oxidase [Sigma-Aldrich, G2133-250KU], and 340 units/ml catalase [Sigma-Aldrich, C40-100 MG]) and imaged using a ANDOR IXON3 Ultra DU897 EMCCD camera on a Nikon Ti inverted microscope with a 100 × 1.49 NA TIRF objective. Images were acquired using TIRF illumination settings calculated to give a depth of illumination between 100 and 130 nm and images were collected at frame rate (about 15 millisecond exposure time were using a 256 × 256 pixel area of the camera chip) using the sequential illumination setting of the STORM module in Nikon Elements software. Laser power was adjusted so that 50 to 350 localization events were recorded per channel in each 256 × 256 pixel area frame. Acquisition was stopped once 1–3 million localization events were recorded. The STORM images were analyzed using the General Analysis tool set in elements. Following image segmentation and contour mapping, the fraction of mitochondria associated with a lysosome was determined by the analysis of the minimum distance between TOMM20 and its most proximal LAMP1 cluster signal.

MTT assay

MTT assays were performed as a measurement of cell metabolism and survival to oxidative stress insult. MEFs were

seeded at 4,000 cells/well onto 96-well plates. After 48 h, the cells were replenished with fresh culture medium containing increasing concentrations (0–500 μm) of H_20_2 (Sigma, 323,381) for 16 h. After treatment, cell viability was determined by a modified version of the MTT assay. The assay was carried out by discarding the cell culture medium and replacing with 100 μl of fresh culture medium containing 5.0 mg/ml MTT (Millipore-Sigma, M5655) for 4 h at 37°C. Next, the cells were solubilized with 100 μl of a solution containing 50% dimethylformamide and 20% SDS (pH: 4.7), for 16 h. Absorbance (560) nm was measured using a microplate reader (SpectroMax 250; Molecular Devices Corp., Sunnyvale,Ca).

Lysosomal isolation and purity control

The Lysosome Isolation Kit (Sigma, LYSIS01) was used for lysosome enrichment according to the manufacturer's instructions with slight modifications. Cells were harvested and washed with ice-cold PBS before centrifugation at 500 g for 10 min. The pellet was then resuspended in 1X extraction buffer and homogenized with a 10-ml Potter-Elvehjem tissue grinder (DWK Life Sciences, 358,039). The samples were centrifuged at 1000 g for 10 min. The post-nuclear supernatant (PNS) was transferred to a new centrifuge tube, and aliquots (200 μl) were kept for subsequent quality control. The samples were further centrifuged at 20,000 g for 20 min and the pellets were resuspended in a 0.25 M sucrose (Sigma, S4189) using pellet pestle. The crude lysosomal fraction containing a mixture of mitochondria, lysosomes, peroxisomes and endoplasmic reticulum was incubated with 8 mM $CaCl_2$ (Sigma, C2052) followed by centrifugation for 10 min at 5000 g to precipitate mitochondria and the ER. The final supernatant was spun down at 17,000 g for 20 min and the final pellet containing lysosomes was resuspended in 500 μl of reaction buffer (10 mM MOPS, pH 7.3, 0.25 M sucrose, 5.4 μM of cysteine [Pierce, 44,889], 1 mM DTT). The lysosome fraction was devoid of ER and mitochondria according to the quality control performed using HSPA5 and TOMM20 as respective markers.

HEX/β-Hexosaminidase assay

Lysosomal integrity was validated by comparative study of HEX/β-Hexosaminidase activity for intact lysosomes with 10% Triton X-100-lysed lysosomes. HEX/β-Hexosaminidase activity was observed using the membrane impermeant fluorogenic substrate 4-methylumbelliferyl-N-acetyl-β-glucosaminide dehydrate (Sigma, M2133) [3], 12 μg of lysosomes with or without Triton X-100 was used in the assay. Substrate was added to the lysosomal supernatant and kept at 37°C for 15 min. After incubation, the rection was stopped with a solution composed of 2 M Na_2C0_3 (Sigma, 144–55-8), 1.1 M glycine (Fisher Bioreagents, BP381-1), pH 10.2 in H_20 and fluorescence measured in a SpectraMax Gemini EM fluorometer (Molecular Devices) (Ex/Em 365/450 nm). Only lysosomes with an integrity of >85% were used in subsequent assays.

CMA assay

In CMA reactions, 25 μg of purified lysosomes were mixed with 2 μg of purified recombinant GAPDH (Millipore-Sigma, SRE0024) and then incubated for 30 min at 37°C. In each reaction, 10 μl of "6× energy regenerating system" (60 mM $MgCl_2$, 60 mM ATP, 12 mM phosphocreatine, 30 μg creatine phosphokinase, in 0.25 M sucrose, pH 7.4), 0.6 μg HSPA8/HSC70 (Enzo Life Science, ADI-SPP-751-D) were added and the reaction volume was brought to 60 μl with reaction buffer (10 mM MOPS, pH 7.3, 0.25 M sucrose, 5.4 μM cysteine, 1 mM DTT). Control conditions were run in parallel in reactions with no lysosomes, no energy regenerating system or in the presence of protease inhibitors (Sigma, 11,836,170,001). The reactions were incubated at 37°C for 30 min. A fraction of the CMA reaction was then mixed with sample buffer and then boiled at 95°C for 5 min, followed by western blot analysis of rGAPDH.

Measurement of mitochondrial membrane potential

Mitochondrial membrane potential was quantified for MEF cells by detecting the extent of uptake of the potentiometric dye, TMRE (Invitrogen, 2,201,622). TMRE intensity was normalized with MitoTracker Deep Red which is taken up by mitochondria independently of membrane potential. WT, *ctns*$^{-/-}$ and DYNC1LI2 expressing *ctns*$^{-/-}$ cells plated on coverslips were incubated with MitoTracker Deep Red (100 nM) for 15 min at 37°C. They were then incubated with a nonquenching level of TMRE (50 nM) for another 15 min at 37°C. The TMRE staining solution was then washed off and cells were fixed with 4% PAF. ZESIS oil objective (63X) was used to acquire images. Laser light intensities and detector gains were chosen to keep the signal intensities from both MitoTracker Deep Red and TMRE below the saturation levels even at the highest detection levels. Mitochondrial potential per unit mass was assessed as a ratio of the TMRE/MitoTracker Deep red signal. Image analysis was performed by using ImageJ.

Measurement of intracellular ROS accumulation

The cell permeable CellROX Deep Red (ThermoFisher, C10448) detects reactive oxygen species (ROS) in living cells. CellROX Deep Red dye is non-fluorescent in its reduced state but exhibits bright fluorescence when oxidized (excitation/emission maxima at 640/665 nm). CellROX Deep Red was added to WT, *ctns*$^{-/-}$ and DYNC1LI2-reconstituted *ctns*$^{-/-}$ cells at a final concentration of 5 μM and the cells were then incubated for 30 min at 37°C. Subsequently, the medium was removed, and the cells were washed three times with PBS and fixed with 4% PAF. The resulting fluorescence was analyzed using Zeiss LSM 880 laser-scanning confocal microscope attached to a Zeiss Observer Z1 microscope at 21°C, using a 63x oil Plan Apo, 1.4-numerical aperture objective.

Quantitative RT-PCR

RNA was isolated from wild type, *ctns*$^{-/-}$, DYNC1LI2-reconstituted *ctns*$^{-/-}$ cells, and sh*Dync1li2* expressing WT

mouse fibroblasts cells using the RNeasy mini-kit for RNA purification (QIAGEN, 74,104), which includes gDNA-eliminator columns. A total of 100 ng of RNA for each cell line was reverse-transcribed (RT) using iScript cDNA Synthesis Kit (Bio-Rad, 170–8891). Quantitative RT-PCR was performed using QuantiTect SYBR green PCR mix (Bio-Rad, 172–5271), with the following primer mixes: Mm*Dync1li2*-forward-CGGCGACCTGACAAGTGAA, Mm*Dync1li2*-reverse-TGCAGCGTGTGTGATCGTC, Hs*DYNC1LI2*-forward-TACAAGGAGCTGAGCATGGC, Hs*DYNC1LI2*-reverse-GTCGTGGACCAGCTTTCTCA, Mm*Lamp2a*-forward-GCAGTGCAGATGAAGACAAC, Mm*Lamp2a*-reverse- AGTATGATGGCGCTTGAGAC, Mm*Actb*-forward-CATTGTTACCAACTGGGACG, Mm*Actb*- reverse-CAGAGGCATACAGGGACAG, Hs*ACTB*-Forward – GTCATTCCAAATATGAGATGCGT, Hs*ACTB*-Reverse-GCTATCACCTCCCCTGTGTG.

Statistical analysis

Data are presented as mean, and error bars correspond to standard errors of the means (SEMs) unless otherwise indicated. Statistical significance was determined using the unpaired Student's t-test using GraphPad InStat (version 3) or Excel software, and graphs were made using GraphPad Prism (version 6) software. Further details of the analysis are described on the corresponding Figure Legend.

Acknowledgments

Supported by fellowships from the Cystinosis Research Foundation to FR and JZ, by the National Institutes of Health grant numbers: R01HL088256, R01AR070837, R01DK110162 and R21EY028642 to S.D.C, and R01-DK090058 and R01-NS108965 for S.C.

Disclosure statement

No potential conflict of interest was reported by the author(s).

Funding

This work was supported by the Cystinosis Research Foundation [CRFS-2020-001]; Cystinosis Research Foundation [CRFS-2017-001]; National Institutes of Health [R01NS108965]; National Institutes of Health [R01AR070837]; National Institutes of Health [R01HL088256]; National Institutes of Health [R21EY028642]; National Institutes of Health [R01DK110162]; National Institutes of Health [R01DK090058].

ORCID

Sergio D. Catz http://orcid.org/0000-0002-1873-0277

References

[1] Town M, Jean G, Cherqui S, et al. A novel gene encoding an integral membrane protein is mutated in nephropathic cystinosis. Nat Genet. 1998;18(4):319–324.
[2] Kalatzis V. Cystinosin, the protein defective in cystinosis, is a H +-driven lysosomal cystine transporter. EMBO J. 2001;20 (21):5940–5949.
[3] Napolitano G, Johnson JL, He J, et al. Impairment of chaperone-mediated autophagy leads to selective lysosomal degradation defects in the lysosomal storage disease cystinosis. EMBO Mol Med. 2015;7(2):158–174.
[4] Andrzejewska Z, Nevo N, Thomas L, et al. Cystinosin is a component of the vacuolar H+-ATPase-ragulator-rag complex controlling mammalian target of rapamycin complex 1 signaling. J Am Soc Nephrol. 2016;27(6):1678–1688.
[5] Rega LR, Polishchuk E, Montefusco S, et al. Activation of the transcription factor EB rescues lysosomal abnormalities in cystinotic kidney cells. Kidney Int. 2016;89(4):862–873.
[6] Gahl WA, Thoene JG, Schneider JA. Cystinosis. N Engl J Med. 2002;347(2):111–121.
[7] Da Silva V, Zurbrügg R, Lavanchy P, et al. Long-term treatment of infantile nephropathic cystinosis with cysteamine. N Engl J Med. 1985;313(23):1460–1463.
[8] Cherqui S, Courtoy PJ. The renal Fanconi syndrome in cystinosis: pathogenic insights and therapeutic perspectives. Nat Rev Nephrol. 2017;13(2):115–131.
[9] Cherqui S. Cysteamine therapy: a treatment for cystinosis, not a cure. Kidney Int. 2012;81(2):127–129.
[10] Vaisbich M, Pache de Faria Guimaraes L, Shimizu M, et al. Oxidative stress in cystinosis patients. Nephron Extra. 2011;1 (1):73–77.
[11] Zhang J, Johnson JL, He J, et al. Cystinosin, the small GTPase Rab11, and the Rab7 effector RILP regulate intracellular trafficking of the chaperone-mediated autophagy receptor LAMP2A. J Biol Chem. 2017;292(25):10328–10346.
[12] Johnson J, Napolitano G, Monfregola J, et al. Upregulation of the Rab27a-dependent trafficking and secretory mechanisms improves lysosomal transport, alleviates endoplasmic reticulum stress, and reduces lysosome overload in cystinosis. Mol Cell Biol. 2013;33(15):2950–2962.
[13] Hook P, Vallee RB. The dynein family at a glance. J Cell Sci. 2006;119(21):4369–4371.
[14] Holzbaur EL, Hammarback JA, Paschal BM, et al. Correction: homology of a 150K cytoplasmic dynein-associated polypeptide with the Drosophila gene Glued. Nature. 1992;360(6405):695.
[15] Holzbaur EL, Vallee RB. DYNEINS: molecular structure and cellular function. Annu Rev Cell Biol. 1994;10:339–372.
[16] King SJ, Bonilla M, Rodgers ME, et al. Subunit organization in cytoplasmic dynein subcomplexes. Protein Sci. 2002;11 (5):1239–1250.
[17] Wang Y, Huynh W, Skokan TD, et al. CRACR2a is a calcium-activated dynein adaptor protein that regulates endocytic traffic. J Cell Biol. 2019;218(5):1619–1633.
[18] Olenick MA, Holzbaur ELF. Dynein activators and adaptors at a glance. J Cell Sci. 2019;132(6):6.
[19] Olenick MA, Tokito M, Boczkowska M, et al. Hook adaptors induce unidirectional processive motility by enhancing the dynein-dynactin interaction. J Biol Chem. 2016;291 (35):18239–18251.
[20] McKenney RJ, Huynh W, Tanenbaum ME, et al. Activation of cytoplasmic dynein motility by dynactin-cargo adapter complexes. Science. 2014;345(6194):337–341.
[21] Mische S, He Y, Ma L, et al. Dynein light intermediate chain: an essential subunit that contributes to spindle checkpoint inactivation. Mol Biol Cell. 2008;19(11):4918–4929.
[22] Perrone CA, Tritschler D, Taulman P, et al. A novel dynein light intermediate chain colocalizes with the retrograde motor for intraflagellar transport at sites of axoneme assembly in chlamydomonas and mammalian cells. Mol Biol Cell. 2003;14 (5):2041–2056.
[23] Purohit A, Tynan SH, Vallee R, et al. Direct interaction of pericentrin with cytoplasmic dynein light intermediate chain contributes to mitotic spindle organization. J Cell Biol. 1999;147(3):481–492.
[24] Bielli A, Thornqvist P-O, Hendrick AG, et al. The small GTPase Rab4A interacts with the central region of cytoplasmic dynein light intermediate chain-1. Biochem Biophys Res Commun. 2001;281(5):1141–1153.

[25] Goncalves JC, Dantas TJ, Vallee RB. Distinct roles for dynein light intermediate chains in neurogenesis, migration, and terminal somal translocation. J Cell Biol. 2019;218(3):808–819.
[26] Grissom PM, Vaisberg EA, McIntosh JR. Identification of a novel light intermediate chain (D2LIC) for mammalian cytoplasmic dynein 2. Mol Biol Cell. 2002;13(3):817–829.
[27] Jones LA, Villemant C, Starborg T, et al. Dynein light intermediate chains maintain spindle bipolarity by functioning in centriole cohesion. J Cell Biol. 2014;207(4):499–516.
[28] Palmer KJ, Hughes H, Stephens DJ. Specificity of cytoplasmic dynein subunits in discrete membrane-trafficking steps. Mol Biol Cell. 2009;20(12):2885–2899.
[29] Schroeder CM, Ostrem JM, Hertz NT, et al. A Ras-like domain in the light intermediate chain bridges the dynein motor to a cargo-binding region. Elife. 2014;3:e03351.
[30] Tan SC, Scherer J, Vallee RB. Recruitment of dynein to late endosomes and lysosomes through light intermediate chains. Mol Biol Cell. 2011;22(4):467–477.
[31] Horgan CP, Hanscom SR, Jolly RS, et al. Rab11-FIP3 links the Rab11 GTPase and cytoplasmic dynein to mediate transport to the endosomal-recycling compartment. J Cell Sci. 2010;123(2):181–191.
[32] Horgan CP, Hanscom SR, Jolly RS, et al. Rab11-FIP3 binds dynein light intermediate chain 2 and its overexpression fragments the Golgi complex. Biochem Biophys Res Commun. 2010;394(2):387–392.
[33] Lee I-G, Olenick MA, Boczkowska M, et al. A conserved interaction of the dynein light intermediate chain with dynein-dynactin effectors necessary for processivity. Nat Commun. 2018;9(1):986.
[34] Kaushik S, Cuervo AM. The coming of age of chaperone-mediated autophagy. Nat Rev Mol Cell Biol. 2018;19(6):365–381.
[35] Kirchner P, Bourdenx M, Madrigal-Matute J, et al. Proteome-wide analysis of chaperone-mediated autophagy targeting motifs. PLoS Biol. 2019;17(5):e3000301.
[36] Cuervo A, Dice J. Regulation of lamp2a levels in the lysosomal membrane. Traffic. 2000;1(7):570–583.
[37] Kaushik S, Bandyopadhyay U, Sridhar S, et al. Chaperone-mediated autophagy at a glance. J Cell Sci. 2011;124(4):495–499.
[38] Kiffin R, Christian C, Knecht E, et al. Activation of chaperone-mediated autophagy during oxidative stress. Mol Biol Cell. 2004;15(11):4829–4840.
[39] Zhang J, He J, Johnson JL, et al. Chaperone-mediated autophagy upregulation rescues megalin expression and localization in cystinotic proximal tubule cells. Front Endocrinol (Lausanne). 2019;10:21.
[40] Scherer J, Yi J, Vallee RB. PKA-dependent dynein switching from lysosomes to adenovirus: a novel form of host–virus competition. J Cell Biol. 2014;205(2):163–177.
[41] Kaushik S, Cuervo A. Chaperone-mediated autophagy. Methods Mol Biol. 2008;445:227–244.
[42] Malkus K, Ischiropoulos H. Regional deficiencies in chaperone-mediated autophagy underlie α-synuclein aggregation and neurodegeneration. Neurobiol Dis. 2012;46(3):732–744.
[43] Yan W, Frank CL, Korth MJ, et al. Control of PERK eIF2 kinase activity by the endoplasmic reticulum stress-induced molecular chaperone P58IPK. Proc Natl Acad Sci USA. 2002;99(25):15920–15925.
[44] Fusakio ME, Willy JA, Wang Y, et al. Transcription factor ATF4 directs basal and stress-induced gene expression in the unfolded protein response and cholesterol metabolism in the liver. Mol Biol Cell. 2016;27(9):1536–1551.
[45] Harding HP, Zhang Y, Zeng H, et al. An integrated stress response regulates amino acid metabolism and resistance to oxidative stress. Mol Cell. 2003;11(3):619–633.
[46] Youle RJ, Narendra DP. Mechanisms of mitophagy. Nat Rev Mol Cell Biol. 2011;12(1):9–14.
[47] Bellomo F, Signorile A, Tamma G, et al. Impact of atypical mitochondrial cyclic-AMP level in nephropathic cystinosis. Cell Mol Life Sci. 2018;75(18):3411–3422.
[48] Heeman B, Van den Haute C, Aelvoet S-A, et al. Depletion of PINK1 affects mitochondrial metabolism, calcium homeostasis and energy maintenance. J Cell Sci. 2011;124(7):1115–1125.
[49] Suen D-F, Norris KL, Youle RJ. Mitochondrial dynamics and apoptosis. Genes Dev. 2008;22(12):1577–1590.
[50] Gaide Chevronnay HP, Janssens V, Van Der Smissen P, et al. Time course of pathogenic and adaptation mechanisms in cystinotic mouse kidneys. J Am Soc Nephrol. 2014;25(6):1256–1269.
[51] Kaushik S, Cuervo A. Methods to monitor chaperone-mediated autophagy. Methods Enzymol. 2009;452:297–324.
[52] Johansson M, Rocha N, Zwart W, et al. Activation of endosomal dynein motors by stepwise assembly of Rab7–RILP–p150Glued, ORP1L, and the receptor βlll spectrin. J Cell Biol. 2007;176(4):459–471.
[53] Nevo N, Chol M, Bailleux A, et al. Renal phenotype of the cystinosis mouse model is dependent upon genetic background. NephrolDialTransplant. 2010;25(4):1059–1066.
[54] Irizarry RA, Hobbs B, Collin F, et al. Exploration, normalization, and summaries of high density oligonucleotide array probe level data. Biostatistics. 2003;4(2):249–264.
[55] Johnson JL, He J, Ramadass M, et al. Munc13-4 is a Rab11-binding protein that regulates Rab11-positive vesicle trafficking and docking at the plasma membrane. J Biol Chem. 2016;291(7):3423–3438.